

STATISTICAL CHARACTERIZATION OF THE
POINT SPREAD FUNCTION (PSF) OF A
TURBULENCE DEGRADED IMAGING SYSTEM

A THESIS

SUBMITTED TO THE DEPARTMENT OF ELECTRICAL AND
ELECTRONICS ENGINEERING
AND THE INSTITUTE OF ENGINEERING AND SCIENCES
OF BILKENT UNIVERSITY
IN PARTIAL FULFILLMENT OF THE REQUIREMENTS
FOR THE DEGREE OF
MASTER OF SCIENCE

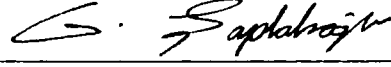
By
M. Fatih Erdoğ
February 1993

QC
880.4
.T8
E73
1993

B01036

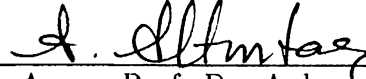
QC
880.4
.T8
E73
1993

I certify that I have read this thesis and that in my opinion it is fully adequate, in scope and in quality, as a thesis for the degree of Master of Science.



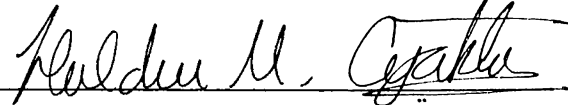
Assist. Prof. Dr. Gürhan Şaplakoglu(Principal Advisor)

I certify that I have read this thesis and that in my opinion it is fully adequate, in scope and in quality, as a thesis for the degree of Master of Science.



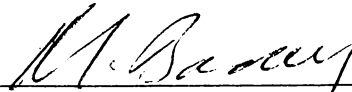
Assoc. Prof. Dr. Ayhan Altıntaş

I certify that I have read this thesis and that in my opinion it is fully adequate, in scope and in quality, as a thesis for the degree of Master of Science.



Assist. Prof. Dr. Haldun M. Özaktas

Approved for the Institute of Engineering and Sciences:



Prof. Dr. Mehmet Baray
Director of Institute of Engineering and Sciences

ABSTRACT

STATISTICAL CHARACTERIZATION OF THE POINT SPREAD FUNCTION (PSF) OF A TURBULENCE DEGRADED IMAGING SYSTEM

M.Fatih Erden

M.S. in Electrical and Electronics Engineering

Supervisor: Assist. Prof. Dr. Gürhan Şaplakoğlu

February 1993

In this thesis, the effect of atmospheric turbulence on an incoherent imaging system is analyzed. The combination of the atmosphere and the imaging system is modelled as a linear system with a stochastic point spread function (PSF). The mean and the covariance of the PSF are evaluated and plotted for a variety of system parameters and atmospheric conditions. The results predicted by this work are shown to be in very good agreement with experimental results published in the literature.

Keywords : Atmospheric turbulence, atmospheric imaging, PSF

ÖZET

M.Fatih Erden

Elektrik ve Elektronik Mühendisliği Bölümü Yüksek Lisans

Tez Yöneticisi: Yard. Doç. Dr. Gürhan Şaplakoğlu

Şubat 1993

Bu tezde, atmosferik türbülansın eşevresiz (incoherent) görüntüleme sistemleri üzerindeki etkisi analiz edilmiştir. Görüntüleme sistemi ile atmosfer, bir doğrusal stokastik nokta yayılım fonksiyonu, NYF (Point Spread Function, PSF) ile modellenmiştir. NYF'nin ortalama değeri ve korelasyonu hesaplanıp, çeşitli sistem parametreleri ve atmosfer şartları için grafikleri verilmiştir. Bu çalışmanın sonuçları, yayınlanan deneysel veriler ile çok iyi derecede uyumaktadır.

Anahtar Kelimeler : Atmosferik türbülans, atmosferik görüntüleme, NYF

ACKNOWLEDGEMENT

I would like to thank to Assoc. Prof. Dr. Gürhan Şaplakoğlu for his supervision, guidance, suggestions and encouragement through the development of this thesis.

I want to express my special thanks to S. Halit Oğuz for his help in the image processing laboratory.

It is a pleasure to express my thanks to all my friends for their valuable discussions and helps, and to my family for their encouragement.

I also would like to thank to AGARD and TUBITAK for their support in this research.

TABLE OF CONTENTS

1	INTRODUCTION	1
1.1	Assumptions	2
1.2	Notations and Definitions	3
1.3	Atmospheric Model	4
1.4	Solution of the Wave Equation in a Turbulent Medium	6
1.4.1	Rytov Transformation	7
1.4.2	Extended Hugins-Fresnel Principle	8
2	IMAGING THROUGH TURBULENT ATMOSPHERE	11
2.1	Impulse Response of an Incoherent Atmospheric Imaging System	12
2.2	Statistical Averages of the Impulse Response	14
2.2.1	Mean of the Impulse Response	14
2.2.2	Correlation of the Impulse Response	16
3	RESULTS	18
3.1	Effect of C_n^2 on the Mean Function	18
3.2	Resolution of the Optical System	20
3.3	Effect of κ_0 and κ_m	22

3.4	Shape of the Mean Function	25
3.5	Effect of the Exposure Time	27
3.6	Variance of the System	28
3.7	Covariance of the System	28
4	CONCLUSION	33
	Appendix A	36
	Appendix B	39
	Appendix C	42
	Appendix D	44
	Appendix E	47

LIST OF FIGURES

1.1	<i>Power spectral densities of n_1</i>	5
2.1	<i>Imaging system model used in this thesis</i>	12
2.2	<i>Linear filter model of the imaging system and the atmosphere</i> .	14
2.3	<i>Mean of the PSF as a function of position ($C_n^2 = 10^{-15} m^{-2/3}$, $D = 0.2 m$, $\lambda = 550 nm$, $d_2 = 2.052 m$, $z = 5 km$, $\kappa_0 = 2\pi/3$, $\kappa_m = 2960$, and $m = 1/77$)</i>	15
3.1	<i>The mean of the PSF for different C_n^2 parameters ($D = 0.2 m$, $\lambda = 550 nm$, $d_2 = 2.052 m$, $z = 5 km$, $\kappa_0 = 2\pi/3$, $\kappa_m = 2960$, and $m = 1/77$)</i>	19
3.2	<i>Peak values of the mean of PSF's as a function of C_n^2 ($D = 0.2 m$, $\lambda = 550 nm$, $d_2 = 2.052 m$, $z = 5 km$, $\kappa_0 = 2\pi/3$, $\kappa_m = 2960$, and $m = 1/77$)</i>	21
3.3	<i>R (3.5) as a function of Diameter for different C_n^2 values ($\lambda =$ $550 nm$, $d_2 = 2.052 m$, $z = 5 km$, $\kappa_0 = 2\pi/3$, $\kappa_m = 2960$, and $m = 1/77$)</i>	22
3.4	<i>Normalized means of PSF for different C_n^2 values ($D = 0.2 m$, $\lambda = 550 nm$, $d_2 = 2.052 m$, $z = 5 km$, $\kappa_0 = 2\pi/3$, $\kappa_m = 2960$, and $m = 1/77$)</i>	23
3.5	<i>R' (3.6) as a function of C_n^2 ($D = 0.2 m$, $\lambda = 550 nm$, $d_2 =$ $2.052 m$, $z = 5 km$, $\kappa_0 = 2\pi/3$, $\kappa_m = 2960$, and $m = 1/77$)</i>	24

3.6	R' (3.6) as a function of Diameter for different C_n^2 values ($\lambda = 550\text{ nm}$, $d_2 = 2.052\text{ m}$, $z = 5\text{ km}$, $\kappa_0 = 2\pi/3$, $\kappa_m = 2960$, and $m = 1/77$)	25
3.7	Mean of PSF as a function of position for different x_1 values	26
3.8	Mean of PSF as a function of position for different x_2 values	26
3.9	Curves which fit to mean of the PSF ($C_n^2 = 10^{-15}\text{ m}^{-2/3}$, $D = 0.2\text{ m}$, $\lambda = 550\text{ nm}$, $d_2 = 2.052\text{ m}$, $z = 5\text{ km}$, $\kappa_0 = 2\pi/3$, $\kappa_m = 2960$, and $m = 1/77$)	27
3.10	Variance vs $ \bar{p} $, ($\bar{p} = \bar{p}_A$, $\bar{p}' = \bar{p}'_A = 0$, $C_n^2 = 10^{-15}$, $D = 0.2\text{ m}$, $\lambda = 550\text{ nm}$, $d_2 = 2.052\text{ m}$, $z = 5\text{ km}$, $\kappa_0 = 2\pi/3$, $\kappa_m = 2960$, and $m = 1/77$)	29
3.11	Covariance vs $ \bar{p} $, ($\bar{p} = -\bar{p}_A$, $\bar{p}' = \bar{p}'_A = 0$, $C_n^2 = 10^{-15}$, $D = 0.2\text{ m}$, $\lambda = 550\text{ nm}$, $d_2 = 2.052\text{ m}$, $z = 5\text{ km}$, $\kappa_0 = 2\pi/3$, $\kappa_m = 2960$, and $m = 1/77$)	30
3.12	Covariance vs $ \bar{p} $, ($\bar{p}' = -\bar{p}'_A$, $\bar{p} = \bar{p}_A = 0$, $C_n^2 = 10^{-15}$, $D = 0.2\text{ m}$, $\lambda = 550\text{ nm}$, $d_2 = 2.052\text{ m}$, $z = 5\text{ km}$, $\kappa_0 = 2\pi/3$, $\kappa_m = 2960$, and $m = 1/77$)	31
3.13	Covariance vs $ \bar{p} $, (\bar{p}' and \bar{p}'_A are fixed, $\bar{p} = \bar{p}_A$, $C_n^2 = 10^{-15}$, $D = 0.2\text{ m}$, $\lambda = 550\text{ nm}$, $d_2 = 2.052\text{ m}$, $z = 5\text{ km}$, $\kappa_0 = 2\pi/3$, $\kappa_m = 2960$, and $m = 1/77$)	32
4.1	OTF versus spatial frequency ($1/\text{mm}$), ($\text{height}=50\text{m}$, $C_n^2 = 4.82 \times 10^{-15}\text{ m}^{-2/3}$, $\lambda=550\text{nm}$, $z=11\text{km}$)	34
C.1	$\kappa\Phi_n(\kappa)$ versus κ ($C_n^2 = 10^{-15}\text{ m}^{-2/3}$, $D = 0.2\text{ m}$, $\lambda = 550\text{ nm}$, $d_2 = 2.052\text{ m}$, $z = 5\text{ km}$, $\kappa_0 = 2\pi/3$, $\kappa_m = 2960$, and $m = 1/77$)	41

Chapter 1

INTRODUCTION

The resolution of an ideal, i.e., aberration free, imaging system is determined by the size of its aperture stop. Larger the size of the aperture stop, better the resolution. However, for atmospheric imaging systems this is not always the case, because the atmosphere through which the waves must propagate is a medium with spatially and temporally varying index of refraction, which may have detrimental effects on the resolution.

Our purpose in this thesis is to investigate the effects of the atmosphere on a general imaging system which consists of an aberration free, ideal thin lens of finite size.

The outline of the thesis is as follows; in the *Introduction*, we will state the major limitations of the study, notations and definitions, model of the atmosphere, and available methods in studying atmospheric propagation. In chapter 2, *Imaging Through The Atmosphere*, the combination of the atmosphere and the imaging system will be modelled as a linear system with a stochastic impulse response function which is called *Point Spread Function* (PSF) in optics. The mean, variance and covariance functions of the PSF will be obtained. In the 3rd chapter, these statistics will be interpreted and compared with related work in the literature. The thesis will be concluded in chapter 4 with an overview and some proposals of future work on this subject.

In the published literature, there is very little work done on imaging through turbulent atmosphere under incoherent illumination. Consequently, the main results of this thesis i.e., the first and the second order statistics of the PSF are original contributions. The only published literature that is closely related to our work is [1]. It is shown in chapter 4 that, when compared with [1], the

results obtained in this thesis is in much closer agreement with the experimental data given in [2].

1.1 Assumptions

Throughout this study, it is assumed that the objects of interest either radiate or are illuminated by incoherent light. Such an assumption can also be made for an object that is illuminated by laser light, since the reflected light that is emitted is essentially incoherent when the scale of the irregularities of the object surface is large compared to the coherence length of the light beam [3].

Furthermore, the radiation (or illumination) is assumed to be monochromatic. Practically, this assumption implies the existence of a narrow band filter at the entrance aperture of the imaging system.

It is also assumed that, the scale size (i.e., correlation length) of the turbulence induced inhomogeneities in the index of refraction are much larger than the wavelength of the radiation being used. This assumption eliminates from consideration problems involving imaging through clouds or aerosols, for which the refractive index changes are sharp. This latter class of problems may be referred to as *imaging through turbid media*, whereas we are concerned here with *imaging through turbulent media*. The clear atmosphere of the Earth is the prime example of a *turbulent* medium [4].

Finally, it is assumed that, all parts of the image is subjected to the statistically identical (turbulence induced) deterioration. That is, the statistics of the noise that distorts the image is constant throughout the image plane. A region satisfying the above condition is referred to as an *isoplanatic patch* [5]. In general an image may consist of several isoplanatic patches since the rays that form a certain portion of an image may have propagated through a region of the turbulence having different statistics compared to the region travelled by rays that form a neighboring isoplanatic patch. In the long exposure case (i.e., exposure time $> \frac{1}{1000}$ sec.), the image is assumed to lie within a single isoplanatic patch since the temporal fluctuations of the turbulence average out any statistical differences that may exist over short time intervals. However, the short exposure case (i.e., exposure time $< \frac{1}{1000}$ sec.) consists of several isoplanatic patches. In [5], it is theoretically shown that the seeing limit, which is the resolution limit of the human eye, can resolve the isoplanatic patches.

1.2 Notations and Definitions

The refractive index of the Earth's atmosphere varies over space, time, and wavelength [4] and can be expressed as,

$$n(\bar{r}, t, \lambda) = n_0(\bar{r}, t, \lambda) + n_1(\bar{r}, t, \lambda) \quad (1.1)$$

where n_0 is the deterministic (nonrandom) portion of n , whereas n_1 represents random fluctuations of n about the mean value n_0 . For typical values of n_1 , $|n_1| \ll n_0$ [4].

The deterministic part of the refractive index varies very slowly with time, consequently the time dependence of n_0 can be ignored. Furthermore, the turbulent eddies of the atmosphere have a range of scale sizes much larger than the optical wavelengths, hence the wavelength dependence of n_1 can also be ignored,

$$n(\bar{r}, t, \lambda) = n_0(\bar{r}, \lambda) + n_1(\bar{r}, t) \quad (1.2)$$

Since the time required for light to propagate through the atmosphere is only a small fraction of the temporal fluctuation time of the random refractive index component n_1 , the time dependence of n_1 can be suppressed. When temporal properties are of interest in a given problem, they can be taken into account by invoking the *frozen turbulence* hypothesis [4] (also known as Taylor's hypothesis), which assumes that a given realization of the random structure n_1 drifts across the measurement aperture with constant velocity (determined by the local wind conditions).

Assuming monochromatic radiation and accepting that n_0 is essentially constant over the region of our propagation experiment, the refractive index can be further simplified as,

$$n(\bar{r}) = n_0 + n_1(\bar{r}) \quad (1.3)$$

The statistics of (1.3) is well documented in literature [4]. In our calculations, we will often use the spatial autocorrelation function of n_1 which is defined as,

$$\Gamma_n(\bar{r}_1, \bar{r}_2) = E[n_1(\bar{r}_1)n_1(\bar{r}_2)] \quad (1.4)$$

When n_1 is spatially stationary in three-dimensional space, we say that it is statistically homogeneous, and its autocorrelation function takes the simpler form

$$\Gamma_n(\bar{r}) = E[n_1(\bar{r}_1)n_1(\bar{r}_1 - \bar{r})] \quad (1.5)$$

If n_1 is also assumed to be statistically isotropic in addition to homogeneity, the autocorrelation function comes out to be only a function of $|\bar{r}|$.

The power spectral density of n_1 is the three-dimensional Fourier transform of (1.5),

$$\Phi_n(\bar{\kappa}) = \frac{1}{(2\pi)^3} \int_V \Gamma_n(\bar{r}) e^{-j\bar{\kappa} \cdot \bar{r}} d^3\bar{r} \quad (1.6)$$

where $\bar{\kappa} = (\kappa_x, \kappa_y, \kappa_z)$ is the wavenumber vector and may be regarded as a vector of spatial frequencies with units of radians per meter.

1.3 Atmospheric Model

At optical frequencies the refractive index of air is given by [4]

$$n = 1 + 77.6(1 + 7.52 \times 10^{-3} \lambda^{-2}) \frac{P}{T} \times 10^{-6} \quad (1.7)$$

where λ is the wavelength of light in micrometers, P is the atmospheric pressure in millibars, and T is the temperature in Kelvin. Throughout the literature, it is mentioned that the variations of n with respect to P is negligible compared to the variations with respect to T . Consequently, the random fluctuations of the refractive index n_1 , is caused predominantly by the temperature induced inhomogeneities.

Temperature induced inhomogeneities result in refractive index inhomogeneities, called turbulent eddies, which may be seen as packets of air, each with a characteristic refractive index. The power spectral density, Φ_n , of a homogeneous turbulence, may also be regarded as a measure of the relative abundance of eddies with dimensions $L_X = 2\pi/\kappa_X$, $L_Y = 2\pi/\kappa_Y$, and $L_Z = 2\pi/\kappa_Z$. When the turbulence is isotropic, $\Phi_n(\kappa)$ is a function of only one wavenumber κ , which may be considered as related to eddy size L through $L = 2\pi/\kappa$ [4].

Taking the classic work of Kolmogorov [6] as the basis for modelling turbulence, the power spectral density $\Phi_n(\kappa)$ has the general shape shown in Figure 1.1.

For very small κ (very large scale sizes), the mathematical form for Φ_n is not predicted by the theory, as the geographic and meteorological conditions are of great importance in this region.

For κ larger than some critical wavenumber κ_0 , Φ_n is assumed to be in the *inertial subrange* of the spectrum, where the form of Φ_n is well defined.

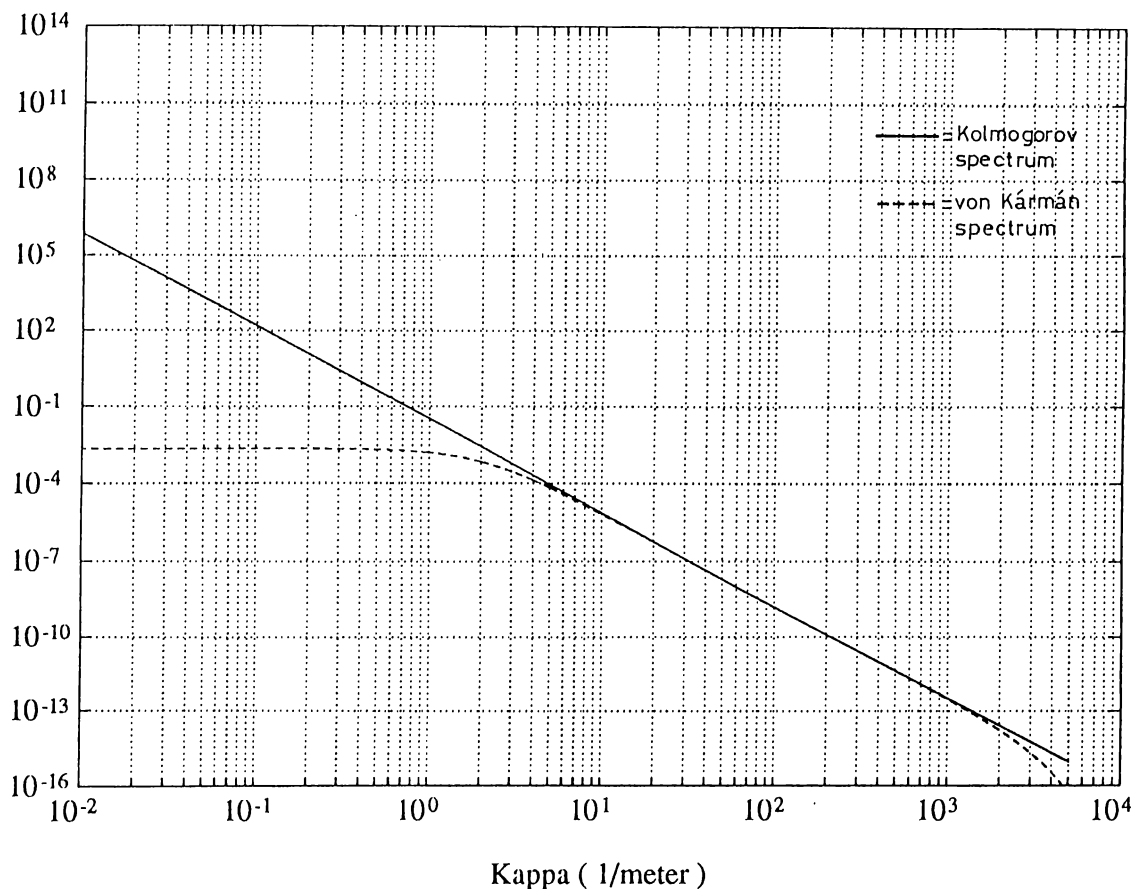


Figure 1.1: Power spectral densities of n_1

Referring to Kolmogorov's work, the form of Φ_n in the inertial subrange is given by

$$\Phi_n(\kappa) = 0.033C_n^2\kappa^{-11/3} \quad (1.8)$$

where C_n^2 is called the *structure constant* of the refractive index fluctuations and serves as a measure of the strength of the turbulence. A detailed summary of Kolmogorov's derivation of $\Phi_n(\kappa)$ can be found in [7].

When κ is beyond another critical value κ_m , Φ_n is assumed to drop rapidly. Tatarski includes the rapid decay of Φ_n for $\kappa > \kappa_m$ by use of the analytical model

$$\Phi_n(\kappa) = 0.033C_n^2\kappa^{-11/3}\exp\left(\frac{-\kappa^2}{\kappa_m^2}\right) \quad (1.9)$$

However, the two spectra given above have nonintegrable poles at the origin. This contradicts with the physical reality because, as mentioned above, the power spectral density for homogeneous and isotropic medium may also be regarded as a measure of the relative abundance of eddies with dimensions $2\pi/\kappa$, so the nonintegrable poles at the origin means infinite amount of eddies with infinite sizes. However, there is finite amount of air that surrounds the Earth. Consequently, there cannot be infinite number of air packets having

extremely large dimensions. This defect is remedied by another model known as the *von Kármán spectrum*, which is expressed as

$$\Phi_n(\kappa) \cong \frac{0.033C_n^2}{(\kappa^2 + \kappa_0^2)^{11/6}} \exp\left(\frac{-\kappa^2}{\kappa_m^2}\right). \quad (1.10)$$

1.4 Solution of the Wave Equation in a Turbulent Medium

Having characterized the statistical properties of the refractive index inhomogeneities in the atmosphere, the effects of these inhomogeneities on the electromagnetic wave propagation are now considered. Specifically, the propagation of a monochromatic electromagnetic wave through the Earth's atmosphere will be investigated. The refractive index of the atmosphere will be assumed to be of the form as given in (1.3).

The atmosphere is assumed to have constant magnetic permeability μ , but space variant dielectric constant ϵ . Hence, using Maxwell's equations, the wave equation, valid in any source-free region, can be written as,

$$\nabla^2 \vec{E} + \left(\frac{wn}{v}\right)^2 \vec{E} + 2\nabla[\vec{E} \cdot \nabla \ln(n)] = 0 \quad (1.11)$$

where \vec{E} is the electric field, v is the velocity of light, n is the position dependent refractive index (1.3).

The last term in this equation introduces coupling between the three components of \vec{E} , and thus corresponds to a depolarization term. It has been well established by past work that in the visible region of the spectrum, this term is completely negligible and can be replaced by zero [7]. Thus (1.11) can be simplified to,

$$\nabla^2 \vec{E} + \left(\frac{wn}{c}\right)^2 \vec{E} = 0 \quad (1.12)$$

This equation is different from the conventional wave equation only through the fact that n^2 in the coefficient of the second term is a random function of position \vec{r} .

Since all the three components of the electric field obey the same wave equation, the vector equation can be replaced by a scalar equation,

$$\nabla^2 U + \left(\frac{wn}{c}\right)^2 U = 0 \quad (1.13)$$

where U can represent E_x, E_y or E_z .

At this point and hereafter, the mean refractive index n_0 is assumed to be unity, which is a very good approximation for the case of atmospheric optical propagation.

An exact solution of (1.13) is not possible, however, several perturbation solutions exist. These can be obtained in two ways. One is to expand U in a series with decreasing magnitudes,

$$U = U_0 + U_1 + U_2 + \dots \quad (1.14)$$

and solve (1.14) for the first few terms. In the other method, the same technique is applied to the exponent of U ;

$$U = \exp(\Psi_0 + \Psi_1 + \Psi_2 + \dots) \quad (1.15)$$

These techniques are referred to as *Born* and *Rytov* approximations respectively.

In Born approximation, the solution for the first 2 terms of the series in (1.14) can be obtained [8]. Consequently, the field can be written as $U = U_0 + U_1$. However, the theoretical results obtained using the Born approximation are not in agreement with the experimental data when the field is represented by the first two terms. The theory is supposed to match the experimental data better when the number of the terms in the series given in (1.14) increases, however, this increases the complexity of the problem considerably.

1.4.1 Rytov Transformation

It has been demonstrated experimentally that the Rytov approximation, unlike the Born approximation, gives fairly accurate results in propagation problems. Consequently, the results of the Rytov method will be used throughout this thesis. As mentioned previously, in the Rytov method, the field is represented with the help of an auxiliary function Ψ , via

$$U(\vec{r}) = \exp[\Psi(\vec{r})] \quad (1.16)$$

A series solution is obtained for $\Psi(\vec{r})$. Using the closed form expressions for Ψ_0 and Ψ_1 , the field is approximated as $U = \exp(\Psi_0 + \Psi_1)$. This technique, known as the Rytov approximation of the first kind, is widely used in propagation problems. There are several theoretical and experimental evidences [8], [4]

which show that for propagation problems, the Rytov approximation of the first kind is superior to the solution when the field is represented by the first two terms of the Born approximation.

When the Rytov approximation of the first kind was first developed, it appeared to yield results in quite good agreement with all the available experimental data, which had been taken over propagation paths of less than 1 km in the atmosphere. However, when the experiments were performed using horizontal propagation paths much greater than 1 km, it was found that [9] the experimental data deviated significantly from the theoretical results obtained by using the Rytov approximation of the first kind. In particular, it was found that, for the Kolmogorov model of the atmosphere, if the propagation path z is such that the condition [9]

$$\sigma_I^2 = 1.23k^{7/6}C_n^2z^{11/6} > 0.3$$

is satisfied, the Rytov approximation of the first kind is no longer valid. This situation is remedied by including Ψ_2 in the expression for the field solution.

However the Rytov method is analytically suitable only for finding basic field solutions like plane wave and spherical wave propagation. For problems involving the propagation of general fields, several methods are available. Among them are the Markov approximation and the Extended Hugen-Fresnel principle.

The Markov approximation is good for giving acceptable results over long paths up to the second order moment of the wave propagating through the turbulent media, but it is quite messy for the fourth and higher order field moments. Moreover, these fourth and higher order field moments cannot be solved in closed form using the Markov approximation [8].

1.4.2 Extended Hugen-Fresnel Principle

The Hugen-Fresnel principle states that the field due to some arbitrary complex disturbance specified over an aperture can be computed for propagation distances that are large compared with the size of the aperture, by superimposing spherical wavelets that radiate from all elements of the aperture. This principle can be extended to an inhomogeneous random medium, which is then referred to as Extended Hugen-Fresnel principle. Extended Hugen-Fresnel principle follows directly from Hugen-Fresnel principle and a field reciprocity

theorem that relates the observation and source points of spherical waves propagating in turbulent media [10].

Using the Extended Hugen-Fresnel principle, the field $U(\bar{p})$ at an observation point \bar{p} due to an arbitrary complex disturbance $U_A(\bar{p}')$ can be written as

$$U(\bar{p}) = -\frac{jk}{2\pi} \int h(\bar{p}, \bar{p}') U_A(\bar{p}') d^2\bar{p}' \quad (1.17)$$

where the integration is carried out over the aperture, k is the optical wavenumber, \bar{p}' and \bar{p} are transverse coordinate vectors in the aperture and observation planes respectively, finally, $h(\bar{p}, \bar{p}')$ is the field of a spherical wave at point \bar{p} , propagating from a point source located at \bar{p}' . The above equation is valid for optical propagation for which the scattered field varies slowly over a wavelength for all propagation distances of interest, and for sufficiently small scattering angles [10].

The expression for $h(\bar{p}, \bar{p}')$ under paraxial conditions is given by,

$$h(\bar{p}, \bar{p}') = z^{-1} \exp[jkz + jk \frac{|\bar{p} - \bar{p}'|^2}{2z} + \Psi(\bar{p}, \bar{p}')] \quad (1.18)$$

where z is the distance between the object plane and the aperture stop. The function $\Psi(\bar{p}, \bar{p}')$ describes the effects of the inhomogeneous medium on the propagation of a spherical waves more specifically, $\Psi(\bar{p}', \bar{p})$ represents the turbulence induced log amplitude and phase perturbation of the field at \bar{p} from a point source at \bar{p}' . Rytov approximation is used to determine $\Psi(\bar{p}, \bar{p}')$.

Unlike the Rytov approximation of the first kind, the term $\Psi(\bar{p}, \bar{p}')$ is modelled as

$$\Psi(\bar{p}, \bar{p}') = \Psi_0(\bar{p}, \bar{p}') + \Psi_1(\bar{p}, \bar{p}') + \Psi_2(\bar{p}, \bar{p}'). \quad (1.19)$$

Up to the second order in n_1 , the addition of $\Psi_2(\bar{p}, \bar{p}')$ makes the solution of the propagating wave conserve energy, predict the correct average field magnitude and give correct phase statistics [11]. One more advantage of adding $\Psi_2(\bar{p}, \bar{p}')$ is that, the Extended Hugen-Fresnel principle yields correct results in strong turbulence regime [8].

On the basis of this principle, the geometry of the problem i.e., the aperture field distribution, can be separated from the propagation problem, which is determined by the propagation of a spherical wave through the turbulent medium. For this reason, the integral equation form (1.17) is quite good for optical applications, and $h(\bar{p}, \bar{p}')$ can be interpreted as the spatial impulse response of the system. Using this interpretation, all the higher order moments of $h(\bar{p}, \bar{p}')$ can be obtained in closed form, utilizing the higher order moments of $\Psi(\bar{p}, \bar{p}')$.

In view of these advantages, the Extended Hugen-Fresnel principle is chosen as the preferred method in calculating and interpreting the higher order field moments.

As mentioned in the very beginning of this chapter, in this thesis, the mean and covariance functions of the PSF of a turbulence degraded imaging system under incoherent illumination are determined and interpreted. To the best of our knowledge, these results are original and have not appeared in the literature previously. The only published literature that is closely related to our work is [1]. It is shown in chapter 4 that, when compared with [1], the results obtained in this thesis is in much closer agreement with the experimental data given in [2].

Chapter 2

IMAGING THROUGH TURBULENT ATMOSPHERE

As mentioned in the *Introduction*, this thesis is concerned with the problem of imaging an extended object through the turbulent atmosphere. For this purpose, the model shown in Figure 2.1 will be used.

In the configuration shown in Figure 2.1, the object is located at a distance of d_1 meters from a thin positive lens of focal length f , and the resulting image is located d_2 meters at the opposite side of the lens.

The distances d_1 , d_2 and the focal length f are related by the well known imaging condition;

$$\frac{1}{d_1} + \frac{1}{d_2} = \frac{1}{f} \quad (2.1)$$

The medium between the image plane and the pupil plane is considered to be turbulence free, and the turbulent medium between the object and the lens is characterized by the power spectral density of the index of refraction fluctuations Φ_n given in (1.10).

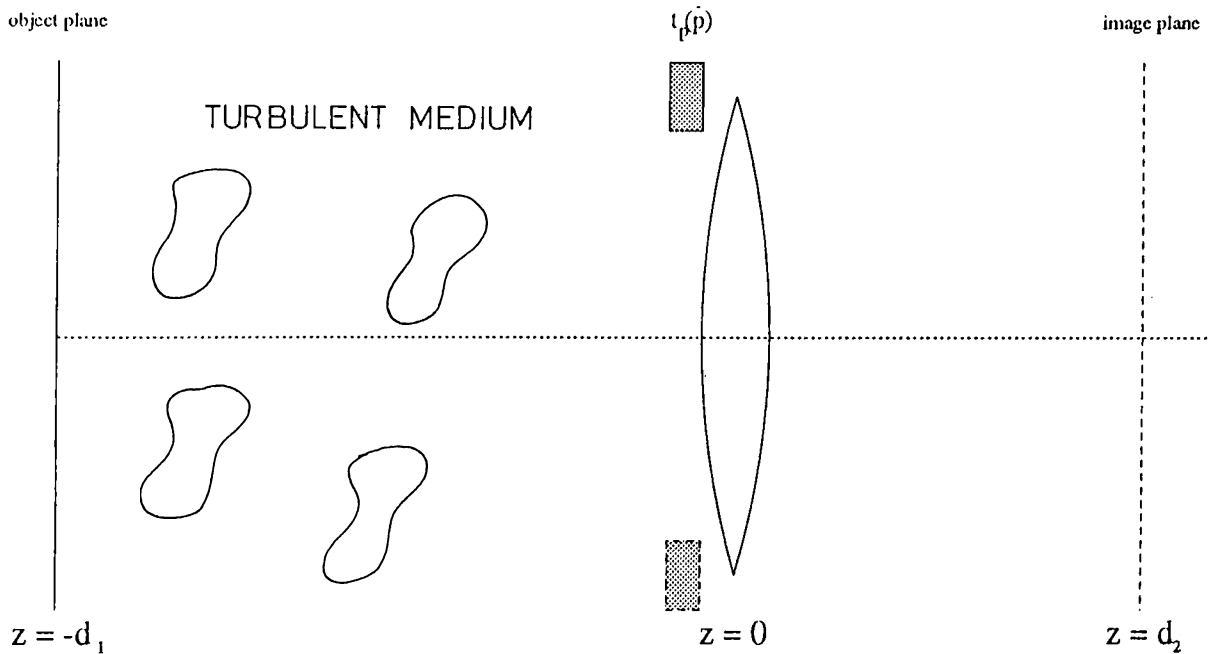


Figure 2.1: *Imaging system model used in this thesis*

2.1 Impulse Response of an Incoherent Atmospheric Imaging System

Referring to Figure 2.1, let $g_{-d_1}(\vec{p})$ be the complex field distribution at the $z = -d_1$ plane. To find the field distribution just before the pupil plane, the Extended Hugen-Fresnel principle (1.17) is used (The terms that don't depend on the transverse coordinates will only have a scaling effect on the resulting expressions, consequently, for simplicity they will be omitted in the rest of this work.);

$$g_{0-}(\vec{p}) = \int d\vec{p}' g_{-d_1}(\vec{p}') e^{jk \frac{|\vec{p}-\vec{p}'|^2}{2d_1} + \Psi(\vec{p}, \vec{p}')} \quad (2.2)$$

which is related to the complex field distribution just after the pupil plane via,

$$g_{0+}(\vec{p}) = g_{0-}(\vec{p}) t_p(\vec{p}) e^{-jk \frac{|\vec{p}|^2}{2f}} \quad (2.3)$$

where $t_p(\vec{p})$ is the pupil function, and $e^{-jk \frac{|\vec{p}|^2}{2f}}$ is the complex amplitude transmittance function of the thin lens.

As the medium between the pupil plane and the image plane is assumed to be turbulent free, the image plane field distribution can easily be found by,

$$g_{d_2}(\vec{p}) = g_{0+} * e^{jk \frac{|\vec{p}|^2}{2d_2}} \quad (2.4)$$

where, $(*)$ represents the convolution operation.

Using the imaging condition (2.1), and combining (2.2), (2.3) and (2.4) yields after some algebra, an expression that relates the image plane field distribution to the object plane distribution [5]

$$u_{d_2}(p) = \int d\bar{p}' u_{-d_1}(p') h(\bar{p}, \bar{p}') \quad (2.5)$$

where,

$$h(\bar{p}, \bar{p}') = \int d\bar{p}'' t_p(\bar{p}'') e^{-j\frac{k}{d_2}(\bar{p}-\bar{p}') \cdot \bar{p}'' + \Psi(\bar{p}'', -\frac{\bar{p}'}{m})} \quad (2.6)$$

$$m = \frac{d_2}{d_1} \quad (2.7)$$

$$u_{d_2}(\bar{p}) = g_{d_2}(\bar{p}) e^{-jk\frac{|\bar{p}|^2}{2d_2}} \quad (2.8)$$

$$u_{-d_1}(\bar{p}) = g_{-d_1}\left(-\frac{\bar{p}}{m}\right) e^{jk\frac{|\bar{p}|^2}{2m^2d_1}} \quad (2.9)$$

In (2.5) the coordinate \bar{p}' is measured using the image scale, i.e., it corresponds to the location of the object on the image plane.

Since $g_{-d_1}(\bar{p})$ is an incoherent field, it is physically meaningful to consider only its intensity distribution [13]. Using the incoherence property of the field, and assuming that the atmospheric turbulence and the field distributions are statistically independent, the intensity distribution at the image plane is found to be,

$$I_{d_2}(\bar{p}) = u_{d_2}(\bar{p}) u_{d_2}^*(\bar{p}) = \int d\bar{p}' I_{-d_1}(\bar{p}') |h(\bar{p}, \bar{p}')|^2 \quad (2.10)$$

where, $h_I(\bar{p}, \bar{p}') = |h(\bar{p}, \bar{p}')|^2$ is defined as the impulse response of the atmospheric imaging system usually referred to as the Point Spread Function (PSF).

Consequently, analyzing the effects of the turbulent atmosphere on the imaging system boils down to a linear filtering problem as shown in Figure 2.2. The intensity distribution of the object is considered as the input, and the intensity distribution of the image is considered as the output of the filter whose (spatial) impulse response is $h_I(\bar{p}, \bar{p}')$;

$$h_I(\bar{p}, \bar{p}') = \int d\bar{p}'' \int d\bar{p}''' t_p(\bar{p}'') t_p^*(\bar{p}''') e^{-j\frac{k}{d_2}(\bar{p}-\bar{p}') \cdot (\bar{p}'' - \bar{p}''')} e^{\Psi(\bar{p}'', -\frac{\bar{p}'}{m}) + \Psi^*(\bar{p}''', -\frac{\bar{p}'}{m})} \quad (2.11)$$

where $h_I(\bar{p}, \bar{p}')$ represents the field at \bar{p} resulting from a point source located at \bar{p}' with scaled image plane source coordinate \bar{p}' .

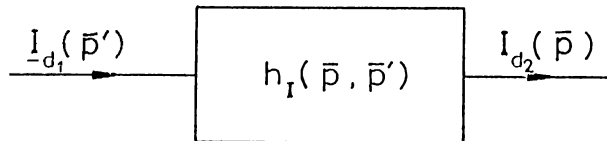


Figure 2.2: *Linear filter model of the imaging system and the atmosphere*

2.2 Statistical Averages of the Impulse Response

Note that (2.11) represents the combined effects of the atmosphere and the imaging system. Consequently, the impulse response is a random quantity. Hence, it is meaningful to talk only about its statistical averages. In the rest of this study, the first and the second order statistics of the impulse response are determined.

2.2.1 Mean of the Impulse Response

Using the above definition of the impulse response of the optical imaging system, and observing that Ψ is the only random variable in (2.11), the mean of the impulse response is,

$$E[h_I(\bar{p}, \bar{p}')] = \int d\bar{p}'' \int d\bar{p}''' t_p(\bar{p}'') t_p^*(\bar{p}''') e^{-j\frac{k}{d_2}(\bar{p}-\bar{p}') \cdot (\bar{p}''-\bar{p}''')} E[e^{\Psi(\bar{p}'', -\frac{\bar{p}'}{m}) + \Psi^*(\bar{p}''', -\frac{\bar{p}'}{m})}] \quad (2.12)$$

The statistical average $E[e^{\Psi(\bar{p}'', -\frac{\bar{p}'}{m}) + \Psi^*(\bar{p}''', -\frac{\bar{p}'}{m})}]$ was evaluated in [10]. Substituting this result into (2.12) yields,

$$E[h_I(\bar{p}, \bar{p}')] = \int d\bar{p}'' \int d\bar{p}''' t_p(\bar{p}'') t_p^*(\bar{p}''') e^{-j\frac{k}{d_2}(\bar{p}-\bar{p}') \cdot (\bar{p}''-\bar{p}''')} e^{-4\pi^2 k^2 z \int_0^1 dt \int_0^\infty d\kappa \kappa \Phi_n(\kappa) [1 - J_0(t|\bar{p}''-\bar{p}'''|\kappa)]} \quad (2.13)$$

where $\Phi_n(\kappa)$ is as defined in (1.6).

It is seen from (2.13) that the mean function depends only on the difference

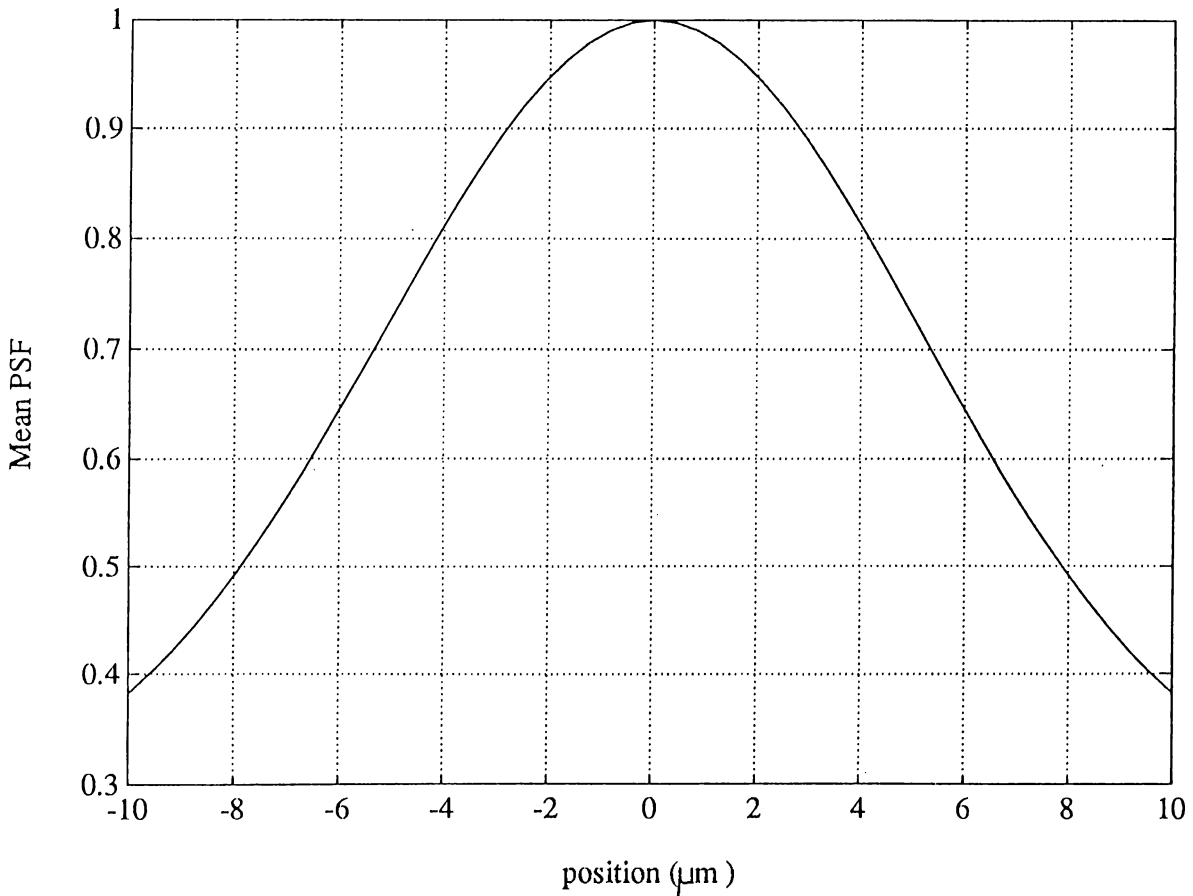


Figure 2.3: Mean of the PSF as a function of position ($C_n^2 = 10^{-15} m^{-2/3}$, $D = 0.2 m$, $\lambda = 550 nm$, $d_2 = 2.052 m$, $z = 5 km$, $\kappa_0 = 2\pi/3$, $\kappa_m = 2960$, and $m = 1/77$)

between \bar{p} and \bar{p}' . i.e.,

$$E[h_I(\bar{p}, \bar{p}')] = E[h_I(\bar{p} - \bar{p}')] \quad (2.14)$$

Thus, it is sufficient to evaluate (2.13) for $\bar{p}' = 0$. Moreover, for a circular pupil function of diameter D , it can be shown that (see Appendix A), the mean function depends only on $p = |\bar{p}|$, and is given by;

$$E[h_I(p)] = \pi D^2 \int_0^D d\varepsilon \varepsilon J_0\left(\frac{2\pi p}{\lambda d_2} \varepsilon\right) \left(\cos^{-1} \frac{\varepsilon}{D} - \frac{\varepsilon}{D} \sqrt{1 - \left(\frac{\varepsilon}{D}\right)^2}\right) e^{-4\pi^2 k^2 z \int_0^1 dt \int_0^\infty d\kappa \kappa \Phi_n(\kappa) [1 - J_0(t\varepsilon\kappa)]} \quad (2.15)$$

The mean of the impulse response as a function of p for typical system and turbulence parameters is shown in Figure 2.3.

2.2.2 Correlation of the Impulse Response

Using (2.11), the correlation function of $h_I(\bar{p}, \bar{p}')$ can be written as,

$$E[h_I(\bar{p}, \bar{p}')h_I(\bar{p}_\Lambda, \bar{p}'_\Lambda)] = \int d\bar{p}'' \int d\bar{p}''' \int d\bar{p}'''' \int d\bar{p}''''' e^{-j\frac{k}{d_2}[(\bar{p}-\bar{p}')\cdot(\bar{p}''-\bar{p}''')+(\bar{p}_\Lambda-\bar{p}'_\Lambda)\cdot(\bar{p}''''-\bar{p}''''')]} \\ t_p(\bar{p}'')t_p^*(\bar{p}''')t_p(\bar{p}''''')t_p^*(\bar{p}''''''') \quad F \quad (2.16)$$

where

$$F = E[e^{\Psi(\bar{p}'', \frac{-\bar{p}'}{m})+\Psi^*(\bar{p}''', \frac{-\bar{p}'}{m})+\Psi(\bar{p}''''', \frac{-\bar{p}'_\Lambda}{m})+\Psi^*(\bar{p}''''''', \frac{-\bar{p}'_\Lambda}{m})}] \quad (2.17)$$

Using the results obtained in Appendix B, the function F is evaluated in Appendix C, and it is expressed as;

$$F = e^{-4\pi^2 k^2 z} \int_0^1 dt \int_0^\infty d\kappa \kappa \Phi_n(\kappa) f_c \quad (2.18)$$

where

$$f_c = 2 - J_0(t|\bar{p}'' - \bar{p}'''|\kappa) - J_0(t|\bar{p}'''' - \bar{p}'''''\kappa) \\ + J_0(|\frac{\bar{p}' - \bar{p}'_\Lambda}{m}(t-1) + t(\bar{p}'' - \bar{p}''')|\kappa) \\ - J_0(|\frac{\bar{p}' - \bar{p}'_\Lambda}{m}(t-1) + t(\bar{p}'' - \bar{p}''''')|\kappa) \\ - J_0(|\frac{\bar{p}' - \bar{p}'_\Lambda}{m}(t-1) + t(\bar{p}'''' - \bar{p}''''')|\kappa) \\ + J_0(|\frac{\bar{p}' - \bar{p}'_\Lambda}{m}(t-1) + t(\bar{p}'''' - \bar{p}''''''')|\kappa) \quad (2.19)$$

It is impossible to progress analytically to simplify the correlation function further. It is also practically impossible to numerically evaluate the correlation function using this expression, because it takes time on the order of several months to obtain the numerical results. For these reasons, the correlation function is further manipulated.

Looking at (2.18), it can be observed that the function F consists of several expressions containing the integral $I(\bar{\alpha}, \bar{\beta})$ where,

$$I(\bar{\alpha}, \bar{\beta}) = \int_0^1 \int_0^\infty d\kappa \kappa \Phi_n(\kappa) J_0(|\bar{\alpha}t + \bar{\beta}|\kappa) \quad (2.20)$$

By choosing $\bar{\alpha}$ and $\bar{\beta}$ properly, (2.18) can be expressed in terms of I . Consequently, approximating I would simplify the numerical evaluation of the correlation function. Using the von Kármán spectrum (1.10) for $\Phi_n(\kappa)$ and defining a new integral variable as $\kappa' = \frac{\kappa}{\kappa_0}$, (2.20) can be written as,

$$I(\bar{\alpha}, \bar{\beta}) = \frac{0.033C_n^2}{\kappa_0^{5/3}} \int_0^1 dt g[\gamma(t)] \quad (2.21)$$

where

$$g[\gamma(t)] = \int_0^\infty d\kappa \kappa \frac{e^{-\kappa^2/(\kappa_m/\kappa_0)^2}}{(\kappa^2 + 1)^{11/6}} J_0[\kappa\gamma(t)] \quad (2.22)$$

and

$$\gamma(t) = |\bar{\alpha}t + \bar{\beta}|\kappa_0 \quad (2.23)$$

After numerically evaluating (2.22) as a function of γ , a polynomial fit can be found for g ,

$$g'(\gamma) = \sum_{i=1}^5 \frac{-2r_i p_i}{\gamma^2 + p_i^2} \quad (2.24)$$

where, the values for r_i and p_i are given in Appendix D. Using (2.24) in (2.20) and evaluating $\int dt$ analytically (see Appendix D), the correlation function is obtained as,

$$E[h_I(\bar{p}, \bar{p}')h_I(\bar{p}_A, \bar{p}'_A)] = \int d\bar{p}'' \int d\bar{p}''' \int d\bar{p}'''' \int d\bar{p}''''' e^{-j\frac{k}{d_2}[(\bar{p}-\bar{p}')\cdot(\bar{p}''-\bar{p}''')+(\bar{p}_A-\bar{p}'_A)\cdot(\bar{p}''''-\bar{p}''''')]} \\ t_p(\bar{p}'')t_p^*(\bar{p}''')t_p(\bar{p}''''')t_p^*(\bar{p}''''''') e^{f_c} \quad (2.25)$$

where

$$f_c = 2I_f(\bar{0}, \bar{0}) - I_f(\bar{p}'' - \bar{p}''', \bar{0}) - I_f(\bar{p}'''' - \bar{p}''''', \bar{0}) \\ + I_f(\bar{p}'' - \bar{p}'''' + \frac{\bar{p}' - \bar{p}'_A}{m}, -\frac{\bar{p}' - \bar{p}'_A}{m}) \\ - I_f(\bar{p}'' - \bar{p}'''' + \frac{\bar{p}' - \bar{p}'_A}{m}, -\frac{\bar{p}' - \bar{p}'_A}{m}) \\ - I_f(\bar{p}'''' - \bar{p}'''''' + \frac{\bar{p}' - \bar{p}'_A}{m}, -\frac{\bar{p}' - \bar{p}'_A}{m}) \\ + I_f(\bar{p}'''' - \bar{p}'''''' + \frac{\bar{p}' - \bar{p}'_A}{m}, -\frac{\bar{p}' - \bar{p}'_A}{m}) \quad (2.26)$$

$I_f(\bar{\alpha}, \bar{\beta})$ is the function that properly fits $I(\bar{\alpha}, \bar{\beta})$ (see Appendix D).

It is possible now to numerically evaluate the correlation function. To speed up the numerical calculation, the integral variables of the correlation expression are modified. The steps and the modified expression for the actual form of the correlation function used in numerical calculations is shown in Appendix E. The plots of the variance and correlation functions are given in chapter 3.

Chapter 3

RESULTS

In this chapter, the first and the second order statistics of the PSF derived in *Chapter 2*, will be interpreted and compared with related work in the literature.

3.1 Effect of C_n^2 on the Mean Function

In section 1.3, the structure constant of the refractive index fluctuations, C_n^2 , was introduced as a measure of the strength of turbulence. Experimental evidence [8], [7] point out that, C_n^2 ranges between 10^{-17} and 10^{-13} , with these values corresponding to exceptionally clear and extremely turbulent conditions respectively.

In Figure 3.1, the mean function, $E[h(\bar{p}, \bar{p}')]$, as given in (2.15) is plotted for different C_n^2 values. It is observed that when C_n^2 (i.e., the strength of turbulence) increases, the peak values decrease and the spread increases. The increase in the spread with increasing turbulence strength is logical since, obviously an imaging system operating at higher levels of turbulence will produce a more blurred image compared to diffraction limited systems. The increase in the spread can be observed more easily in Figure 3.4, which shows the same PSF's plotted in Figure 3.1, with normalized peak values.

Another observation that can be made is the areas under the PSF's shown in Figure 3.1. Note that, the curves as depicted in Figure 3.1 are single dimensional, since they represent a rotationally symmetric impulse response. Consequently, the physically meaningful area under the PSF is $\int dppE[|h(p)|]$,

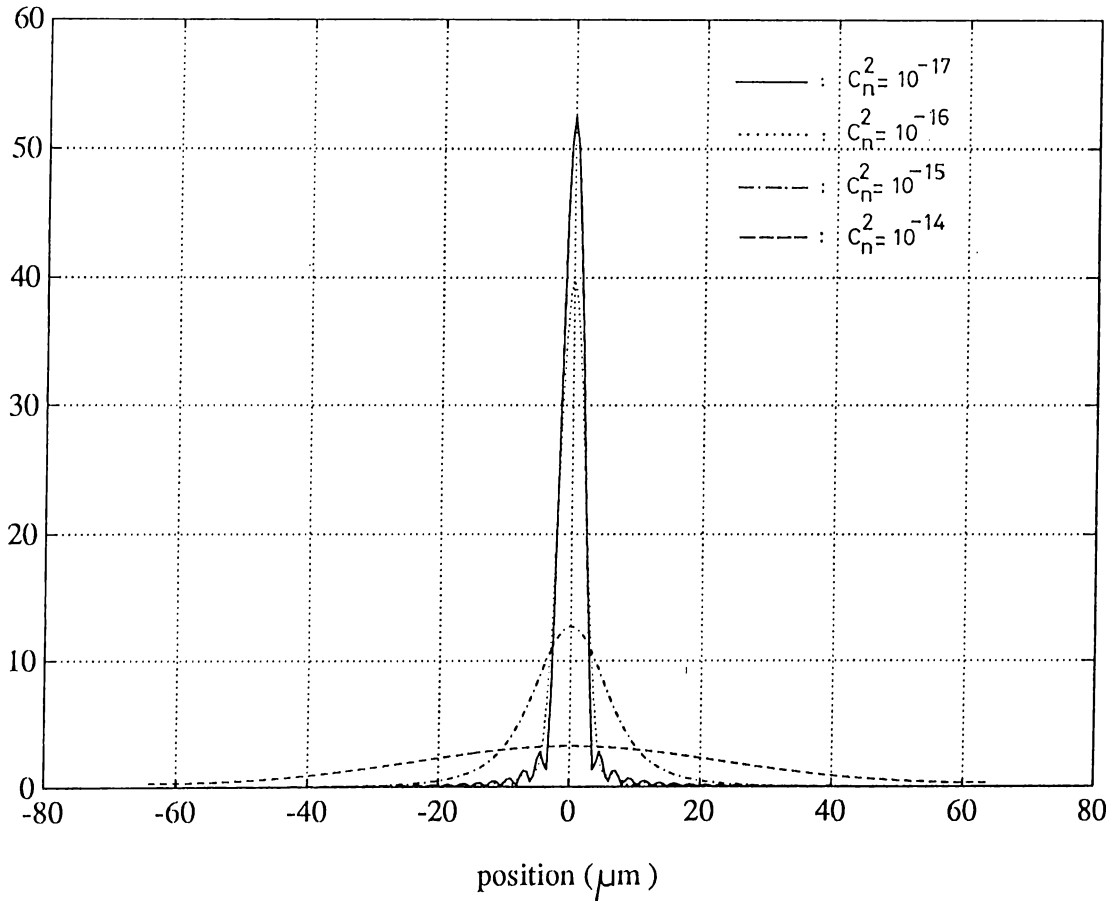


Figure 3.1: The mean of the PSF for different C_n^2 parameters ($D = 0.2 m$, $\lambda = 550 nm$, $d_2 = 2.052 m$, $z = 5 km$, $\kappa_0 = 2\pi/3$, $\kappa_m = 2960$, and $m = 1/77$)

i.e., the volume under the 2-D PSF. Calculation of this volume for each PSF yields a constant value. This fact can also be seen analytically. Using (A.1), the mean function can be written as (assuming a source point at the origin i.e., $\vec{p}' = 0$),

$$E[h_I(\vec{p})] = F\{\Omega(\vec{p}'')\}_{\vec{f}=\frac{\vec{p}}{\lambda d_2}} \quad (3.1)$$

where $F\{.\}$ is the two dimensional Fourier transform operator and,

$$\Omega(\vec{p}'') = e^{-4\pi^2 k^2 z} \int_0^1 dt \int_0^\infty d\kappa \kappa \Phi_n(\kappa) [1 - J_0(t|\vec{p}''|\kappa)] \int d\vec{\eta} t_p(\vec{\eta} + \frac{\vec{\epsilon}}{2}) t_p^*(\vec{\eta} - \frac{\vec{\epsilon}}{2}) \quad (3.2)$$

From the properties of Fourier Transform, we know that

$$\int d\vec{p} h(\vec{p}) = F[h(\vec{p})]_{\vec{f}=0} \quad (3.3)$$

Combining (3.3) with (3.1), we obtain

$$\int d\vec{p} E[h_I(\vec{p})] = \lambda d_2 \Omega(0) = \lambda d_2 \int d\vec{\eta} |t_p(\vec{\eta})|^2 \quad (3.4)$$

As a result of (3.4), the area of the mean function comes out to be invariant under C_n^2 and is directly proportional to the area of the aperture stop. This means that, the total intensity that comes from a point source located at the

origin, is directly proportional to the area of the aperture stop of the imaging system.

This conclusion is consistent with our assumptions, in particular with the paraxial approximation which was used throughout this thesis. Physically, paraxial approximation states that, all the rays emitted by the source are assumed to be travelling close to the z -axis even in strong turbulence regime. Hence, exactly the same portion of the rays emitted by the source are captured by the lens of our imaging system regardless of the strength of turbulence, as long as the width of the PSF is sufficiently small so that it can be contained fully in the image plane. For practical systems, this latter condition is usually met.

The fact that the area of the PSF is constant for a fix aperture diameter D , implies that the peak values of the PSF will be inversely proportional to the turbulence strength. In Figure 3.2, the peak values of the mean functions are shown as a function of C_n^2 . This plot shows that taking C_n^2 between 10^{-17} and 10^{-13} will be enough to model the strength of turbulence of the atmosphere, since outside these limits the variation in C_n^2 do not effect the PSF. This result exactly matches the published results in the literature [8], [7].

3.2 Resolution of the Optical System

In the *Introduction*, it had been pointed out that, ideally, the resolution of an aberration-free optical system is only a function of the size of the optical elements. It has also been pointed out that the medium through which the waves propagate may not be optically perfect, which will drastically effect the resolution. In this section, the resolution of the optical system in the presence of turbulence is discussed.

We will use the following resolution measure;

$$R = 2\pi \int_0^\infty \Omega H(\Omega) d\Omega \quad (3.5)$$

where $H(\Omega)$ is the normalized Fourier transform (OTF) of $E[h_I(\vec{p})]$. This measure is used in [4] in connection with a coherent imaging system. We will use it here for our incoherent imaging system, since the physical implications of the measure in both cases are identical, viz, it is a measure of the volume under the normalized mean functions. Using the above resolution definition, the plot in Figure 3.3 is obtained. This plot shows the resolution as a function

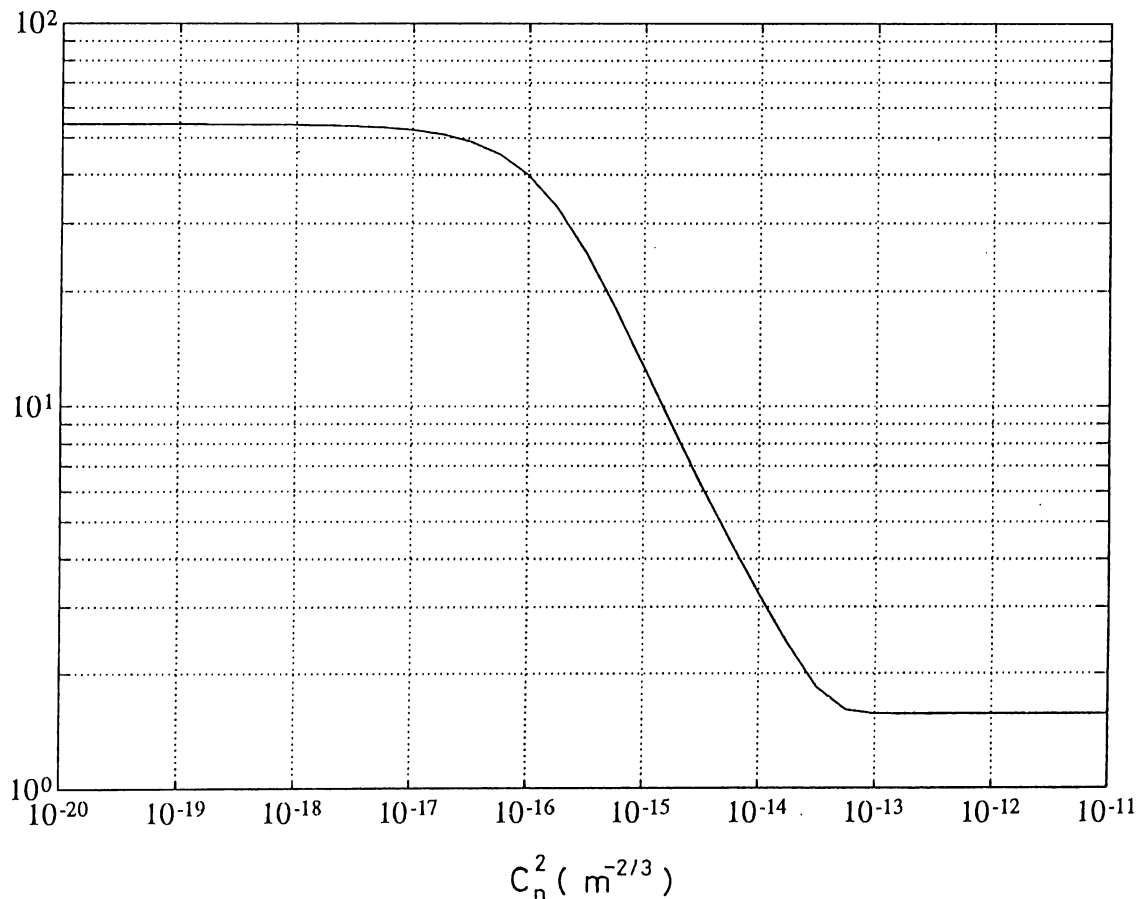


Figure 3.2: Peak values of the mean of PSF's as a function of C_n^2 ($D = 0.2 m$, $\lambda = 550 nm$, $d_2 = 2.052 m$, $z = 5 km$, $\kappa_0 = 2\pi/3$, $\kappa_m = 2960$, and $m = 1/77$)

of the diameter of the pupil function, for a fix C_n^2 .

The plot in Figure 3.3 quantitatively confirms the statement that was made in the beginning of this section, viz the drastic effects of the turbulence on the imaging systems. From the figure it is observed that increasing the diameter increases the resolution up to a maximum value of D . This maximum value, D_{max} , is a function of C_n^2 . Increasing D above D_{max} does not increase the resolution significantly, and eventually, the resolution saturates to a fixed value. As a result, in the presence of turbulence, increasing the size of the aperture above D_{max} , which significantly increases the cost of the system, gains nothing in terms of resolution.

In the previous section, the volume under the PSF for different C_n^2 values, was shown to be constant for a fix aperture diameter D . Consequently, the area can be thought of as a measure indicating the average intensity of the captured image. Consequently, disregarding this information, an indication about the resolution of the system can also be gained by normalizing the peak values of the PSF's and looking at the widths of the resulting functions

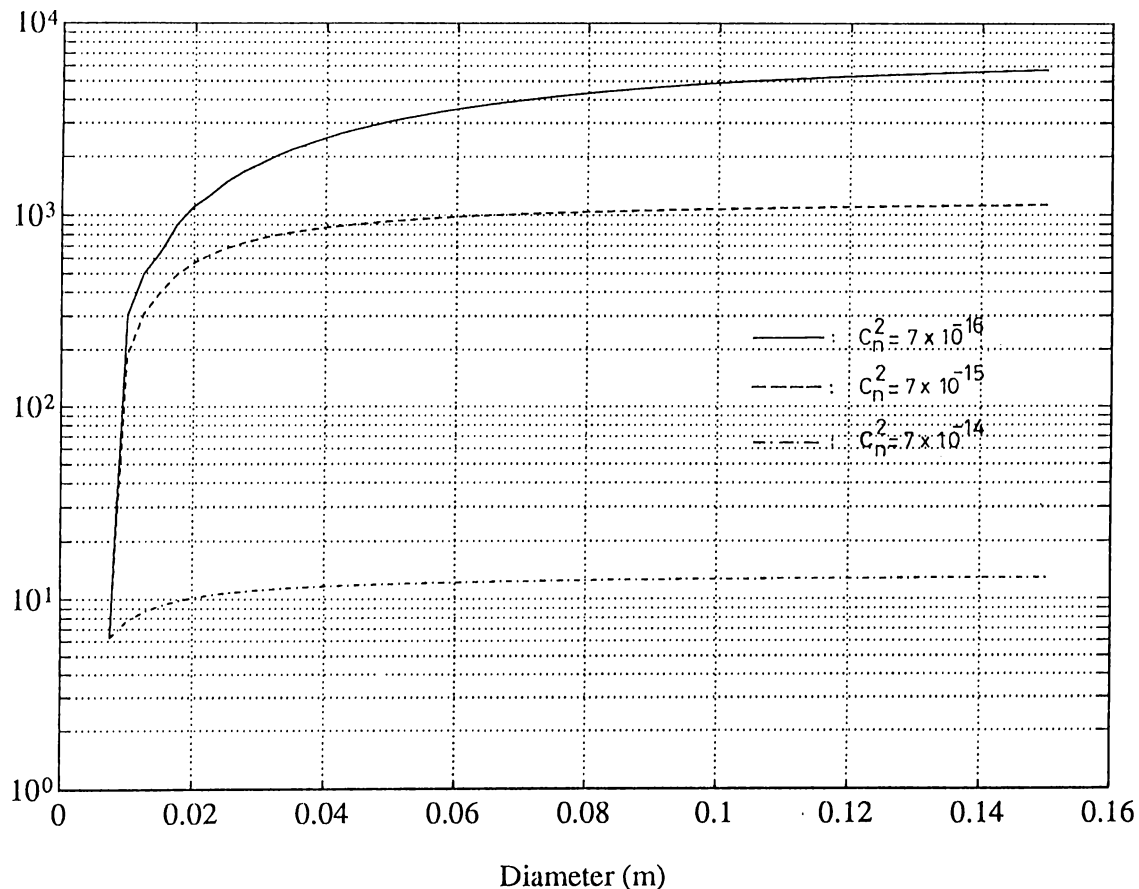


Figure 3.3: R (3.5) as a function of Diameter for different C_n^2 values ($\lambda = 550 \text{ nm}$, $d_2 = 2.052 \text{ m}$, $z = 5 \text{ km}$, $\kappa_0 = 2\pi/3$, $\kappa_m = 2960$, and $m = 1/77$)

For this purpose, a new resolution measure is used;

$$R' = \frac{1}{\int dp p^2 h(p)} \quad (3.6)$$

which mathematically yields a value proportional to the spread of a function.

Figure 3.5 shows R' as a function of C_n^2 . This plot shows the effect of turbulence strength on the resolution of the system. It is also observed that C_n^2 ranges between 10^{-17} and 10^{-13} as deduced previously.

It is also of interest to look at the variation of R' as a function of the diameter of the aperture stop. This is plotted in Figure 3.6, which shows very similar characteristics to Figure 3.3. Hence, the same arguments made for Figure 3.3 can also be applied to Figure 3.6.

3.3 Effect of κ_0 and κ_m

In section 1.3, the *von Kármán spectrum* was given as the most suitable model for the power spectral density of the random fluctuations of the atmosphere.

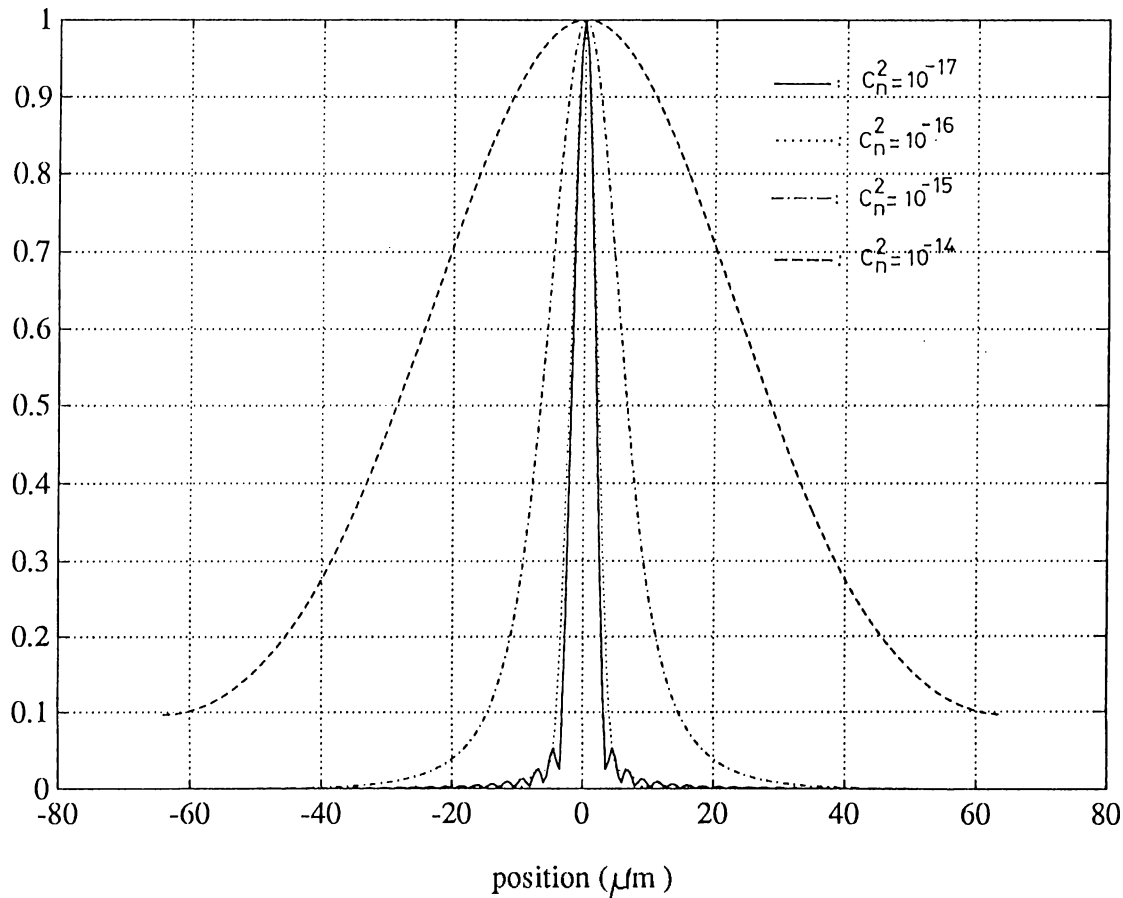


Figure 3.4: Normalized means of PSF for different C_n^2 values ($D = 0.2 m$, $\lambda = 550 nm$, $d_2 = 2.052 m$, $z = 5 km$, $\kappa_0 = 2\pi/3$, $\kappa_m = 2960$, and $m = 1/77$)

In this model, there are 3 important parameters, namely κ_0 , κ_m and C_n^2 , which are necessary in modelling the atmosphere.

Throughout the numerical calculations, it was observed that κ_m had no significant effect on the results. This is because the magnitude of $\Phi_n(\kappa)$ comes very close to zero when κ increases up to κ_m .

However, the effect of κ_0 was found to be significant throughout this thesis. In order to show its effect on the results two important plots are given in Figure 3.7 and 3.8.

In Figure 3.7 the mean of the PSF is plotted as a function of position for different x_1 parameters, where

$$x_1 = \frac{zC_n^2}{\lambda^2\kappa_0^{5/3}} \quad (3.7)$$

It is observed that when x_1 increases (which can also be caused by decreasing κ_0), the peak values of the mean function and the resolution of the system decreases. This behavior can easily be seen from (3.7), since decreasing κ_0 for a fixed C_n^2 is equivalent to increasing C_n^2 (i.e., increasing turbulence strength) for a fixed κ_0 .

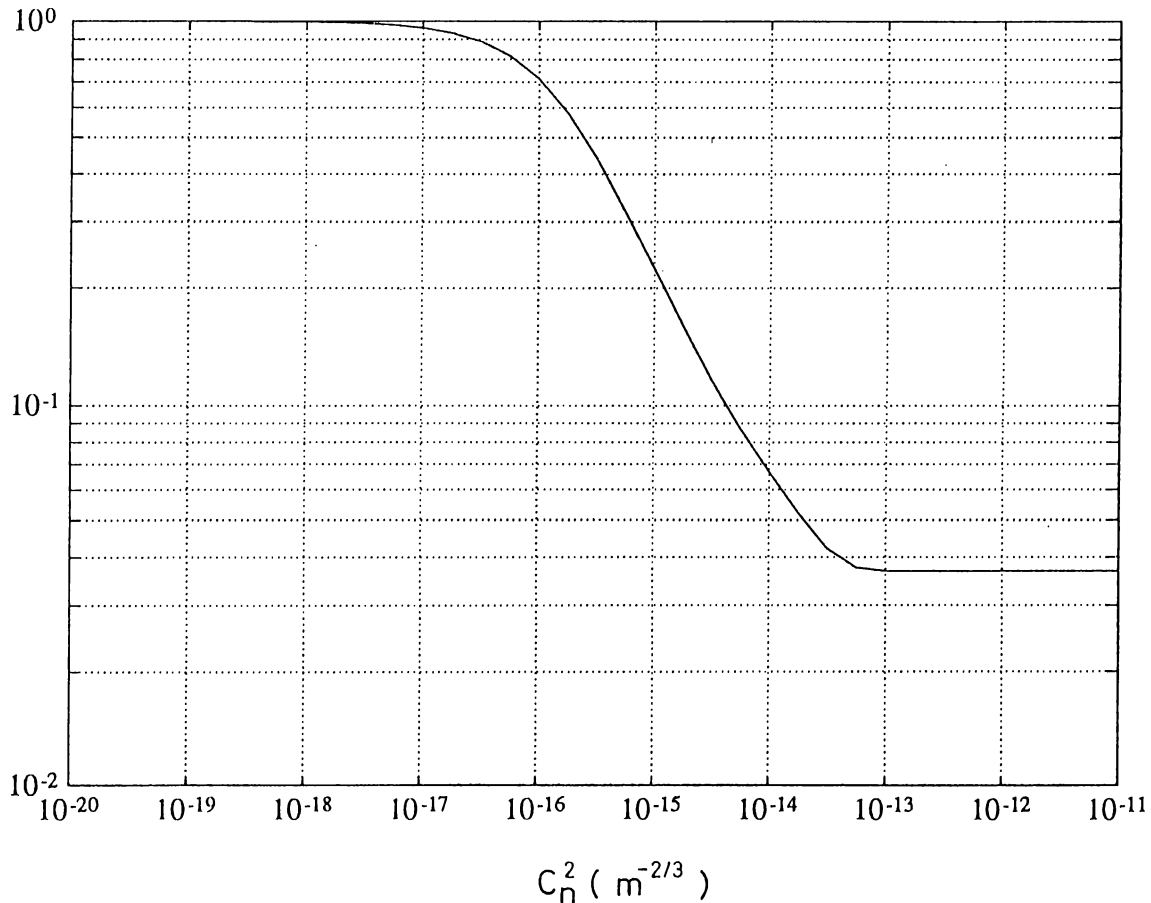


Figure 3.5: R' (3.6) as a function of C_n^2 ($D = 0.2 m$, $\lambda = 550 nm$, $d_2 = 2.052 m$, $z = 5 km$, $\kappa_0 = 2\pi/3$, $\kappa_m = 2960$, and $m = 1/77$)

In Figure 3.8, the mean of the PSF is shown as a function of position for different x_2 parameters, where

$$x_2 = D\kappa_0 \quad (3.8)$$

The effect observed in Figure 3.7 is also observed in this figure. In other words, when x_2 increases (which can also result from increasing κ_0), the peak values of the mean function and the resolution of the system increases.

As κ_0 is roughly proportional to $4\pi/h$, where h is the height above the ground, the above conclusion seems contradictory, because decreasing κ_0 implies imaging at higher altitudes which is known to increase resolution. However, it should be noted that, C_n^2 is very much dependent on h , hence the combined effects of C_n^2 and κ_0 as h is increased, is a significant improvement on resolution.

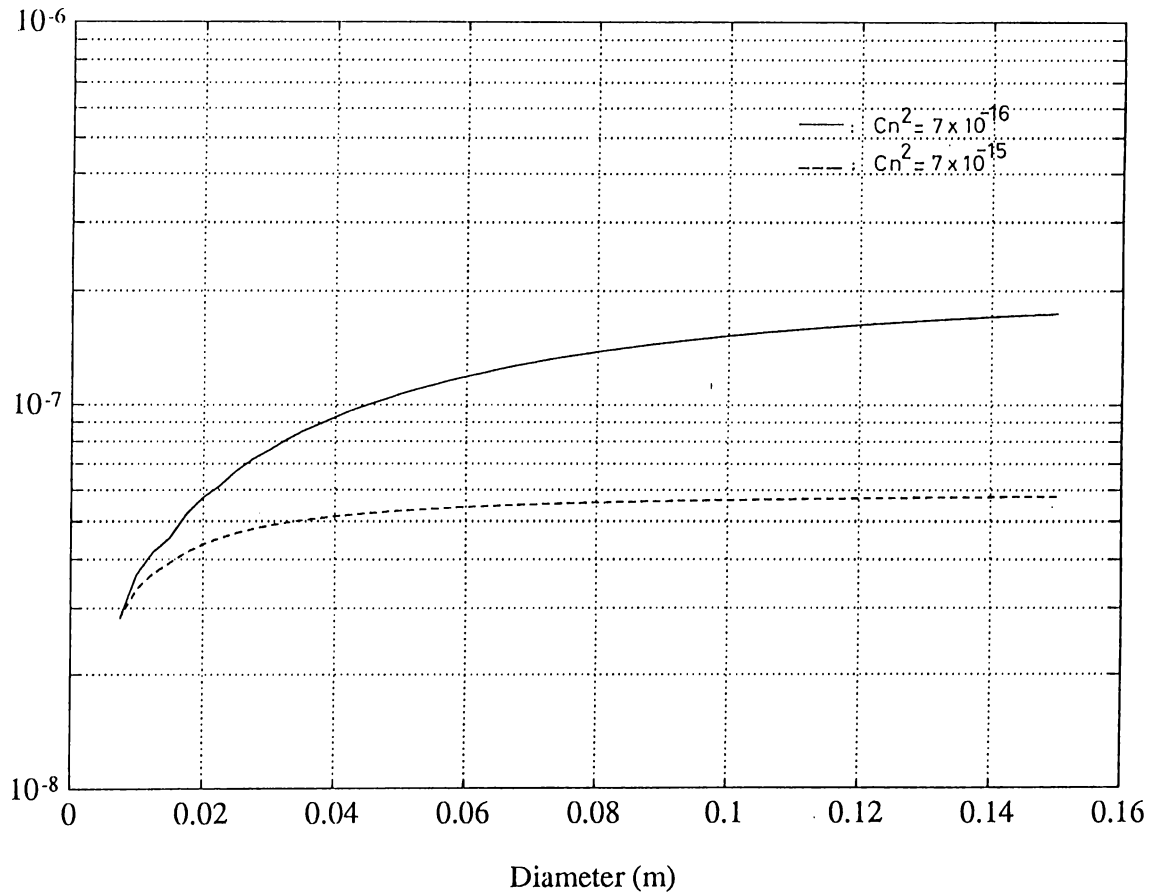


Figure 3.6: R' (3.6) as a function of Diameter for different C_n^2 values ($\lambda = 550 \text{ nm}$, $d_2 = 2.052 \text{ m}$, $z = 5 \text{ km}$, $\kappa_0 = 2\pi/3$, $\kappa_m = 2960$, and $m = 1/77$)

3.4 Shape of the Mean Function

It is also of interest to find an analytically simple curve that fits the mean functions for a given C_n^2 . In the literature, the usual Gaussian function is widely used to model the PSF. However, a function of the form $a_1 e^{a_2 x^{5/3}}$ offers a better numerical fit. Both of these functions are shown in Figure 3.9.

It is also worth analyzing, how the constants a_1 and a_2 in $a_1 e^{a_2 x^{5/3}}$ changes with respect to C_n^2 . The constant a_1 is not important, because it only effects the scaling of the expression. The dependence of a_2 on C_n^2 is given by the following expression;

$$a_2 = a'(m)^e \quad (3.9)$$

where

$$e = \frac{1}{3} \left(\frac{1 - 0.2412m}{0.1242 + 0.0288m - 0.0131m^2} \right) \quad (3.10)$$

and $m = \frac{10^{-15}}{C_n^2}$. Equation (3.10) was obtained by numerical techniques.

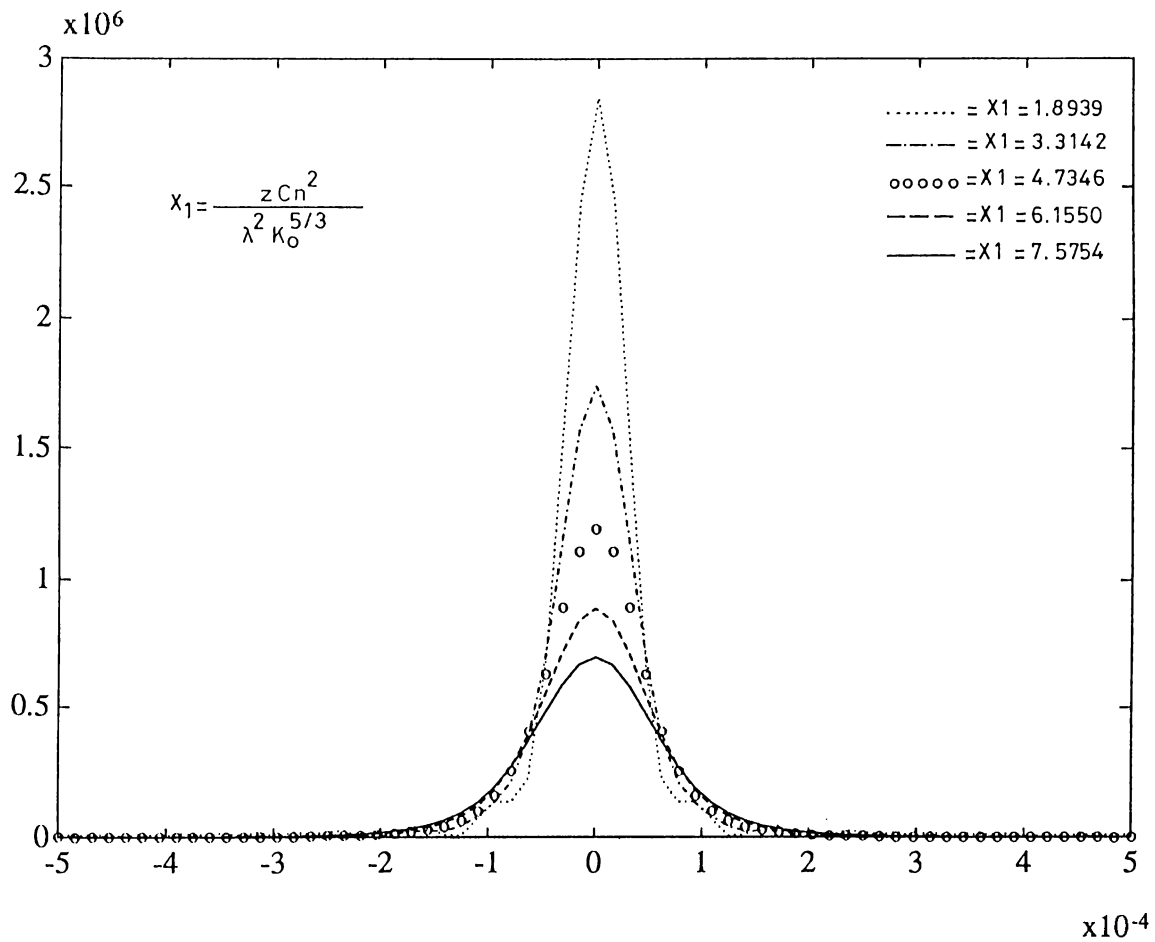


Figure 3.7: Mean of PSF as a function of position for different x_1 values

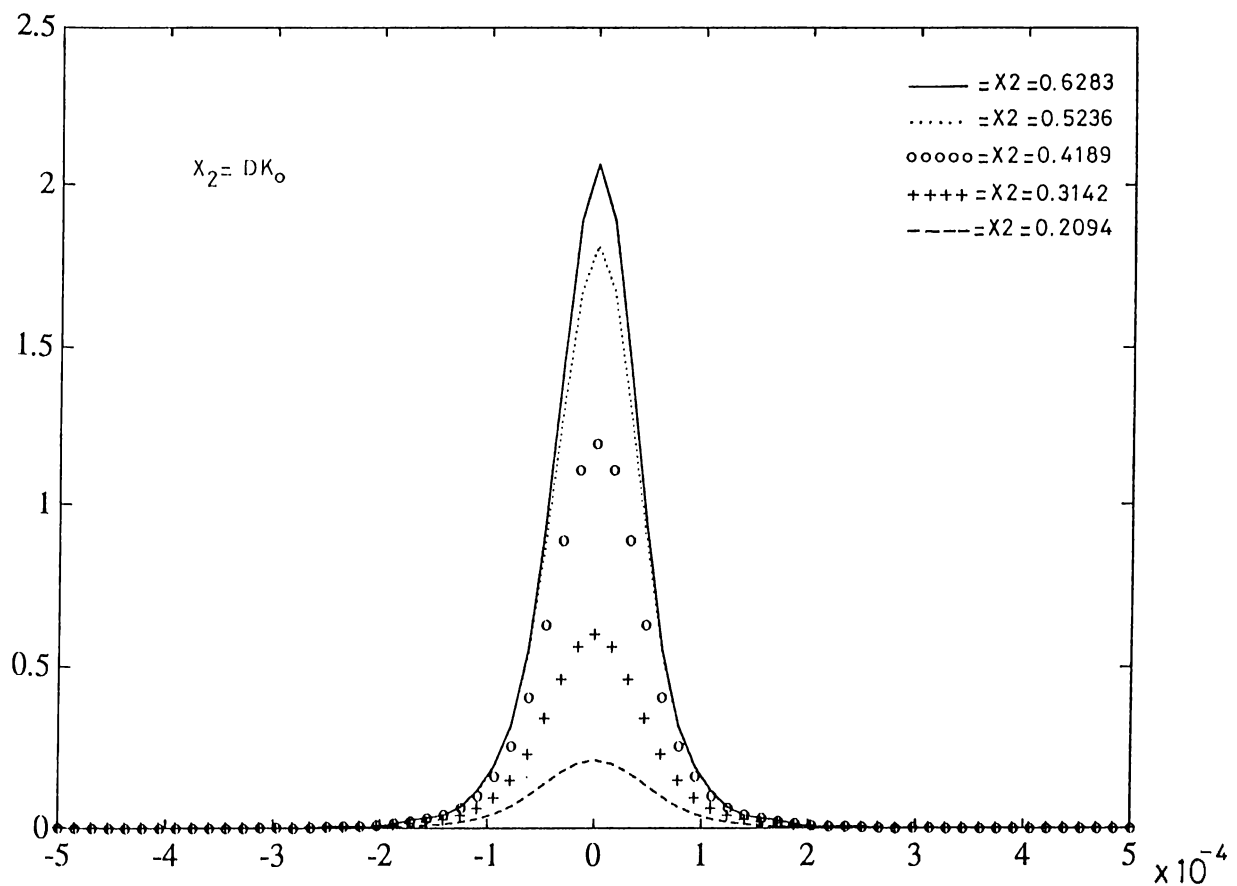


Figure 3.8: Mean of PSF as a function of position for different x_2 values

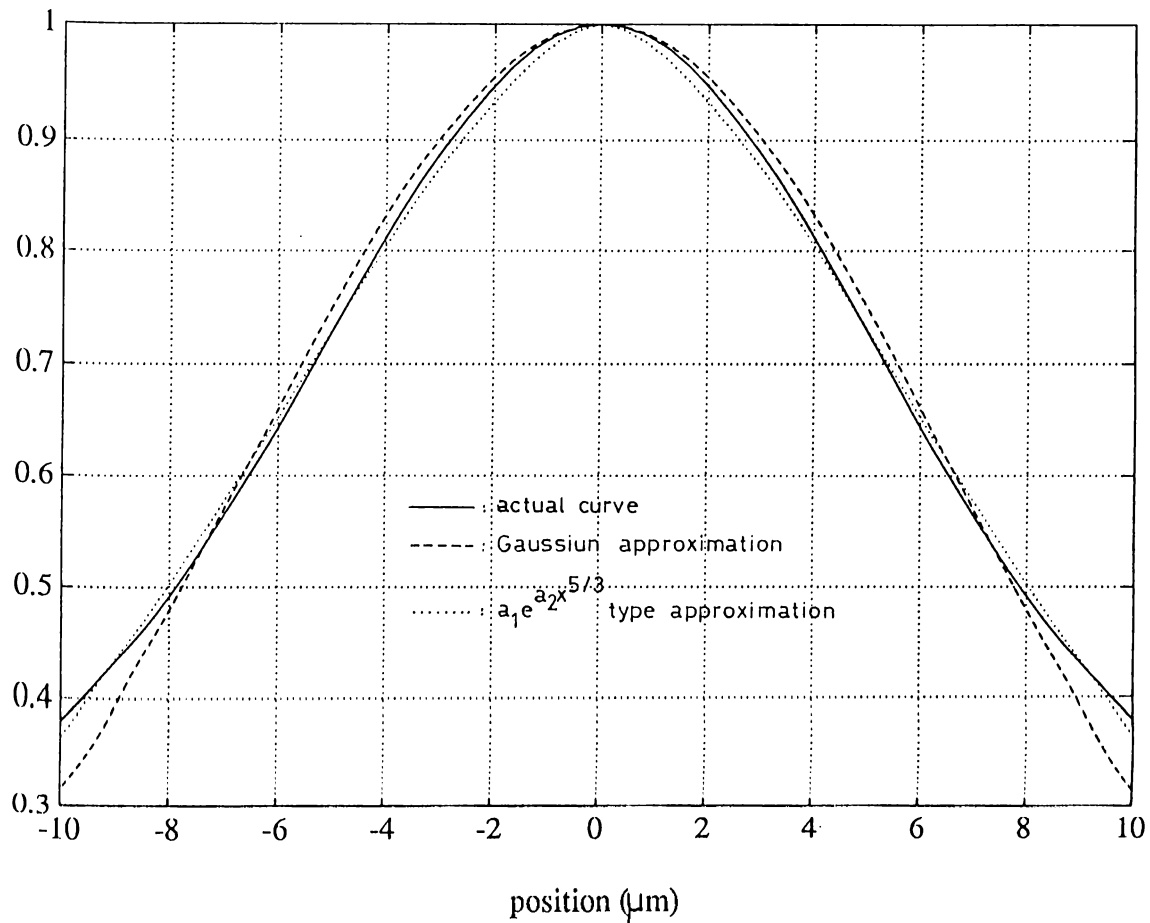


Figure 3.9: Curves which fit to mean of the PSF ($C_n^2 = 10^{-15} \text{ m}^{-2/3}$, $D = 0.2 \text{ m}$, $\lambda = 550 \text{ nm}$, $d_2 = 2.052 \text{ m}$, $z = 5 \text{ km}$, $\kappa_0 = 2\pi/3$, $\kappa_m = 2960$, and $m = 1/77$)

3.5 Effect of the Exposure Time

As pointed out in section 1.1, all the analysis done in this work is true in a particular region of the image plane formed by the rays which have propagated through the same locally homogeneous and isotropic part of the atmosphere. These regions of the image plane which have been subjected statistically to the same deterioration are called *isoplanatic patches*.

In the short-exposure case, the object is considered to lie within a number of isoplanatic patches. However, in [5] it is shown that under typical turbulent conditions, the seeing limit can resolve the isoplanatic patches. This means that the different portions of the image that lie in different isoplanatic patches can be identified. So, the analysis for the short-exposure case (i.e., existence of a number of isoplanatic patches) boils down to analyzing each isoplanatic patch using the techniques developed in this thesis.

In the long-exposure case, because of the time averaging, the image consists of a single isoplanatic patch. So, the tools developed in this thesis can directly be applied to the long-exposure case.

To summarize, the main difference between the short-exposure and the long-exposure cases are the number of isoplanatic patches that constitutes the image. However, this difference creates no problem, and with a little care, the analysis proposed in this thesis can be applied to both of these cases.

3.6 Variance of the System

In this section, an expression for the variance of the PSF is derived. Using the correlation expression (E.6) and the mean expression in (2.13), the following expression for the variance is obtained by setting $\bar{p}' = \bar{p}'_A = 0$ and $\bar{p} = \bar{p}_A$;

$$V(\bar{p}) = \int d\bar{p}'' \int d\bar{p}''' \int d\bar{p}'''' \int d\bar{p}''''' e^{-j\frac{k}{d_2}[\bar{p}(\bar{p}'' - \bar{p}''' + \bar{p}'''' - \bar{p}''''')]} \\ t_p(\bar{p}'') t_p^*(\bar{p}''') t_p(\bar{p}'''') t_p^*(\bar{p}''''') \\ e^{f_m} (e^{f_v} - 1) \quad (3.11)$$

where

$$f_v = I_f(\bar{p}'' - \bar{p}'''' , \bar{0}) - I_f(\bar{p}'' - \bar{p}'''' , \bar{0}) \\ - I_f(\bar{p}''' - \bar{p}'''' , \bar{0}) + I_f(\bar{p}''' - \bar{p}'''' , \bar{0}) \quad (3.12)$$

and

$$f_m = 2I_f(\bar{0}, \bar{0}) - I_f(\bar{p}'' - \bar{p}'''' , \bar{0}) - I_f(\bar{p}''' - \bar{p}'''' , \bar{0}) \quad (3.13)$$

The function $I_f(\bar{\alpha}, \bar{\beta})$ is defined in (D.5).

To simplify the numerical calculations, the covariance function was calculated using the modified version of the correlation function given in (E.6). The result of this calculation is shown in Figure 3.10.

Observation of Figure 3.10 and Figure 2.1 reveals that the noise power (i.e., the variance) is maximum when the signal level (i.e., the mean) is maximum, and it decreases when the signal level starts to decay.

3.7 Covariance of the System

The covariance function is defined as

$$C(\bar{p}, \bar{p}', \bar{p}_A, \bar{p}'_A) = E[h_I(\bar{p}, \bar{p}') h_I(\bar{p}_A, \bar{p}'_A)] - E[h_I(\bar{p}, \bar{p}')] E[h_I(\bar{p}_A, \bar{p}'_A)]$$

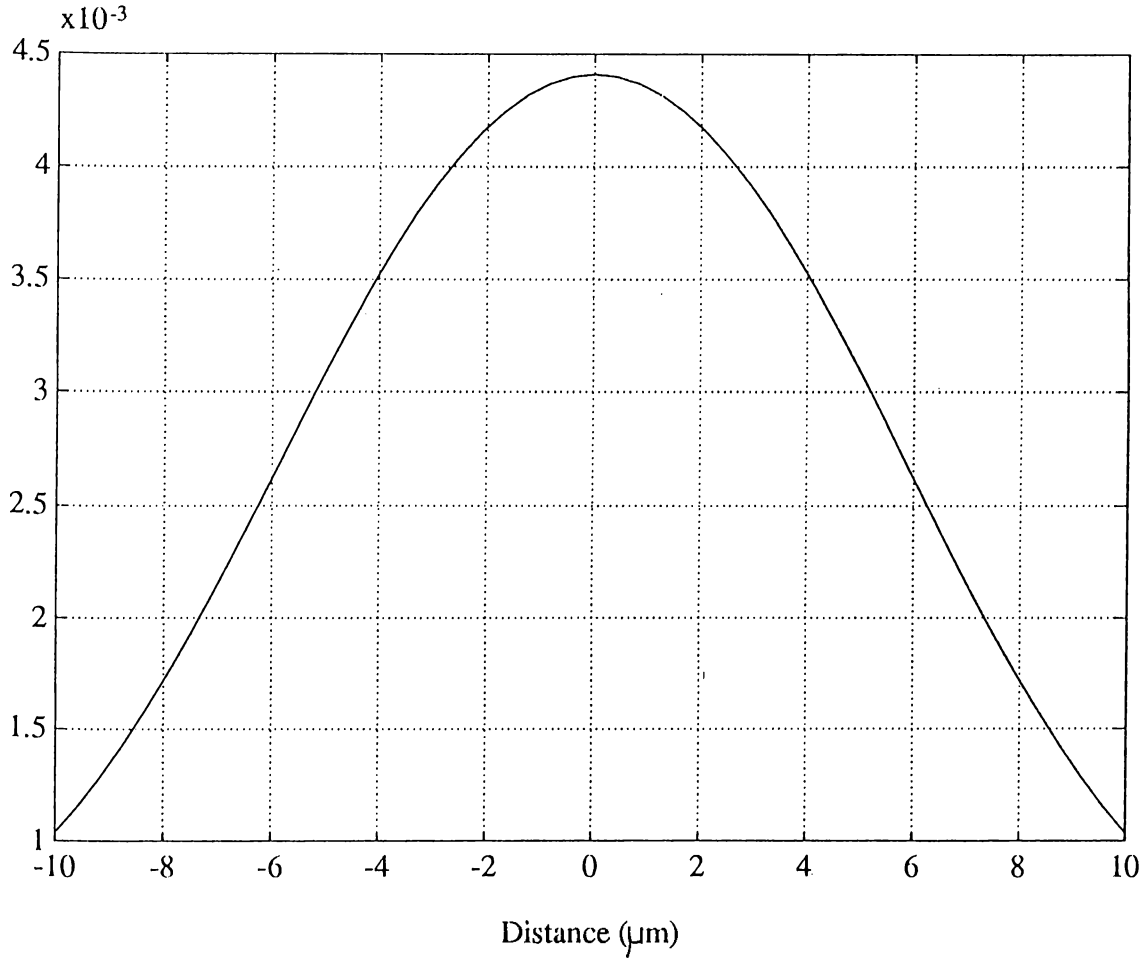


Figure 3.10: Variance vs $|\bar{p}|$, ($\bar{p} = \bar{p}_A$, $\bar{p}' = \bar{p}'_A = 0$, $C_n^2 = 10^{-15}$, $D = 0.2 m$, $\lambda = 550 nm$, $d_2 = 2.052 m$, $z = 5 km$, $\kappa_0 = 2\pi/3$, $\kappa_m = 2960$, and $m = 1/77$)

Using the equations (2.13) and (2.25) together with (D.5), an expression for $C(\bar{p}, \bar{p}', \bar{p}_A, \bar{p}'_A)$ can be obtained;

$$C(\bar{p}, \bar{p}', \bar{p}_A, \bar{p}'_A) = \int d\bar{p}'' \int d\bar{p}''' \int d\bar{p}'''' \int d\bar{p}''''' e^{-j\frac{k}{d_2}[(\bar{p}-\bar{p}')\cdot(\bar{p}''-\bar{p}''')+(\bar{p}_A-\bar{p}'_A)\cdot(\bar{p}''''-\bar{p}''''')]} t_p(\bar{p}'')t_p^*(\bar{p}''')t_p(\bar{p}''''')t_p^*(\bar{p}''''') e^{f_m}(e^{f_c} - 1) \quad (3.14)$$

where

$$f_c = I_f(\bar{p}'' - \bar{p}'''' + \frac{\bar{p}' - \bar{p}'_A}{m}, -\frac{\bar{p}' - \bar{p}'_A}{m}) - I_f(\bar{p}'' - \bar{p}'''' + \frac{\bar{p}' - \bar{p}'_A}{m}, -\frac{\bar{p}' - \bar{p}'_A}{m}) - I_f(\bar{p}''' - \bar{p}'''' + \frac{\bar{p}' - \bar{p}'_A}{m}, -\frac{\bar{p}' - \bar{p}'_A}{m}) + I_f(\bar{p}''' - \bar{p}'''' + \frac{\bar{p}' - \bar{p}'_A}{m}, -\frac{\bar{p}' - \bar{p}'_A}{m}) \quad (3.15)$$

and

$$f_m = 2I_f(0, 0) - I_f(\bar{p}'' - \bar{p}''', 0) - I_f(\bar{p}'''' - \bar{p}''''', 0) \quad (3.16)$$

The covariance function is plotted for several cases which are shown in figures 3.11, 3.12 and 3.13 (The modified version of the correlation function given in

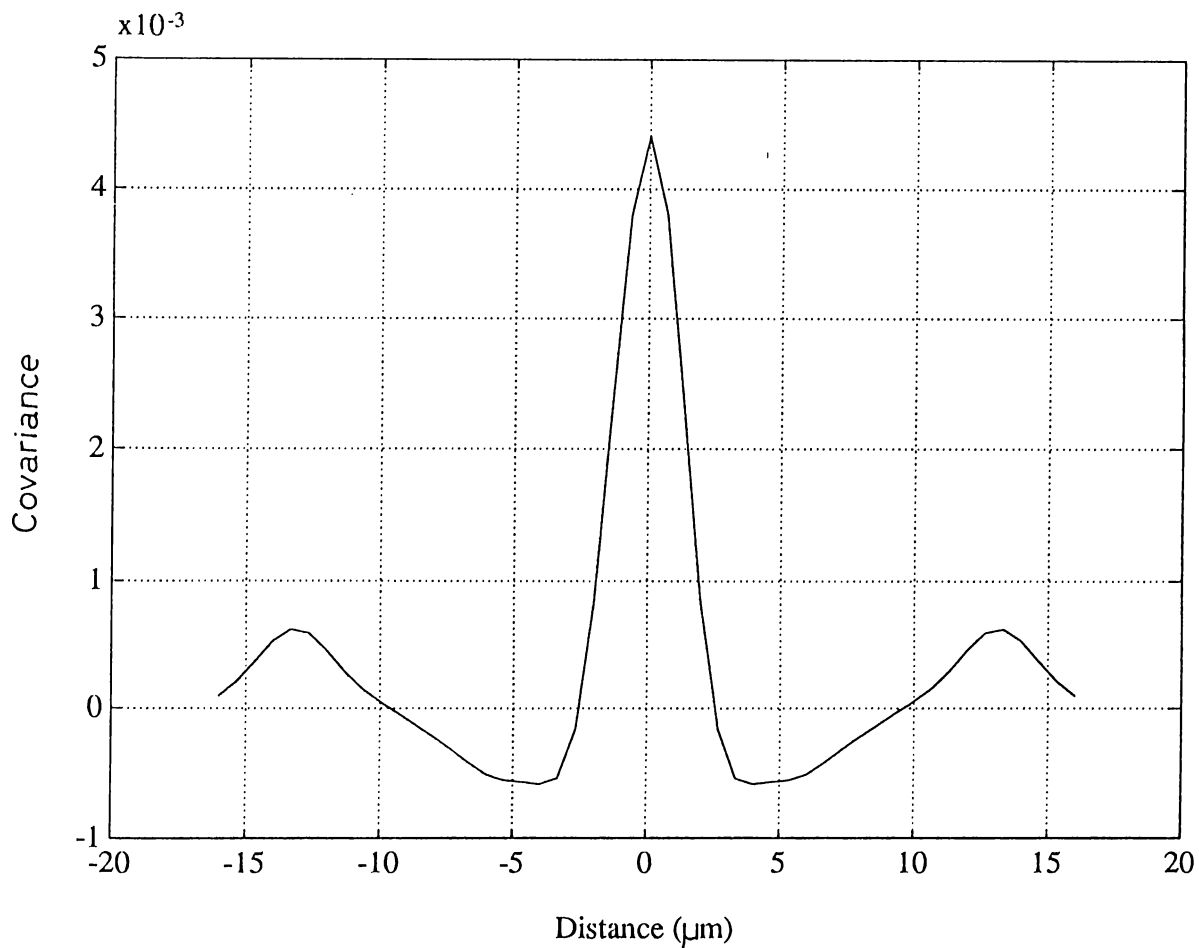


Figure 3.11: Covariance vs $|\bar{p}|$, ($\bar{p} = -\bar{p}_A$, $\bar{p}' = \bar{p}'_A = 0$, $C_n^2 = 10^{-15}$, $D = 0.2 m$, $\lambda = 550 nm$, $d_2 = 2.052 m$, $z = 5 km$, $\kappa_0 = 2\pi/3$, $\kappa_m = 2960$, and $m = 1/77$)

(E.6) is used in order to get the plots). In Figure 3.11 and Figure 3.12 the covariance function is plotted as a function of a single variable.

Figure 3.11 shows the covariance as a function of $|\bar{p}|$ when $\bar{p} = -\bar{p}_A$ and $\bar{p}' = \bar{p}'_A = 0$. In other words, both of the object coordinates are set to zero, and, the distance between the image coordinates are varied. As seen from the figure, the covariance function is maximum when $|\bar{p}| = 0$ (i.e., when the points in the image plane are coincident), and starts to decrease when $|\bar{p}|$ increases (i.e., the distance between \bar{p} and \bar{p}_A increases). This is an expected result because of the definition of the covariance function, viz, it shows that, the correlation between two observation points starts to decrease when the distance between the observation points on the image plane increases.

The above comment also applies to Figure 3.12 which shows the covariance as a function of $|\bar{p}'|$ when $\bar{p}' = -\bar{p}'_A$ and $\bar{p} = \bar{p}_A = 0$. That is, the correlation between the observation points located at fixed distances from each other, starts to decrease when the distance between the source points on the object plane increases.

Figure 3.13 shows the covariance as a function of $\bar{p} = -\bar{p}_A$ when \bar{p}' and \bar{p}'_A

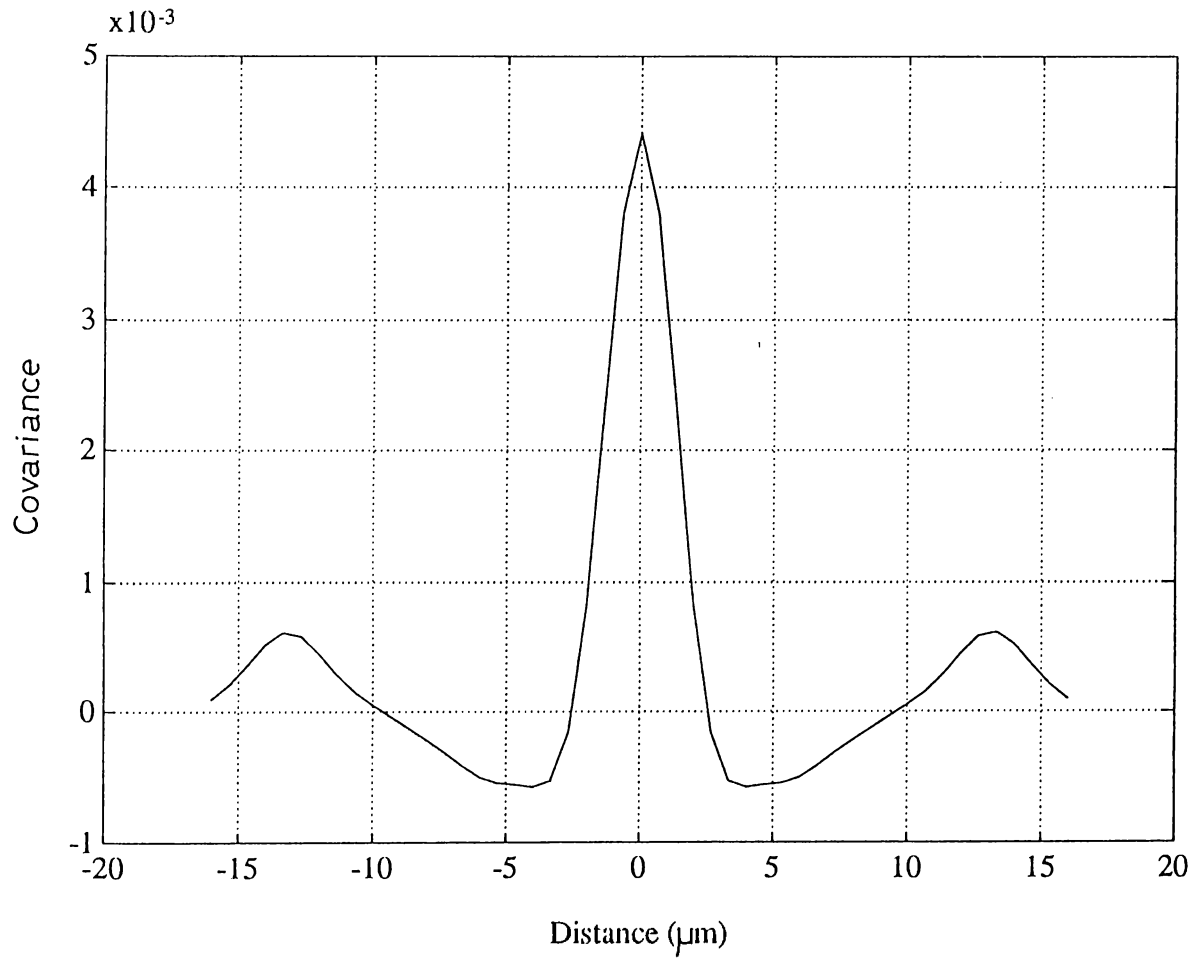


Figure 3.12: Covariance vs $|\bar{p}|$, ($\bar{p}' = -\bar{p}'_A$, $\bar{p} = \bar{p}_A = 0$, $C_n^2 = 10^{-15}$, $D = 0.2 m$, $\lambda = 550 nm$, $d_2 = 2.052 m$, $z = 5 km$, $\kappa_0 = 2\pi/3$, $\kappa_m = 2960$, and $m = 1/77$)

are fixed. This figure indicates that the covariance function is maximum when $\bar{p} = \bar{p}_A$ is in between \bar{p}' and \bar{p}'_A . In other words, the noise is maximum in the image plane, at that point, which corresponds on the object plane to the point in the middle of the source points.

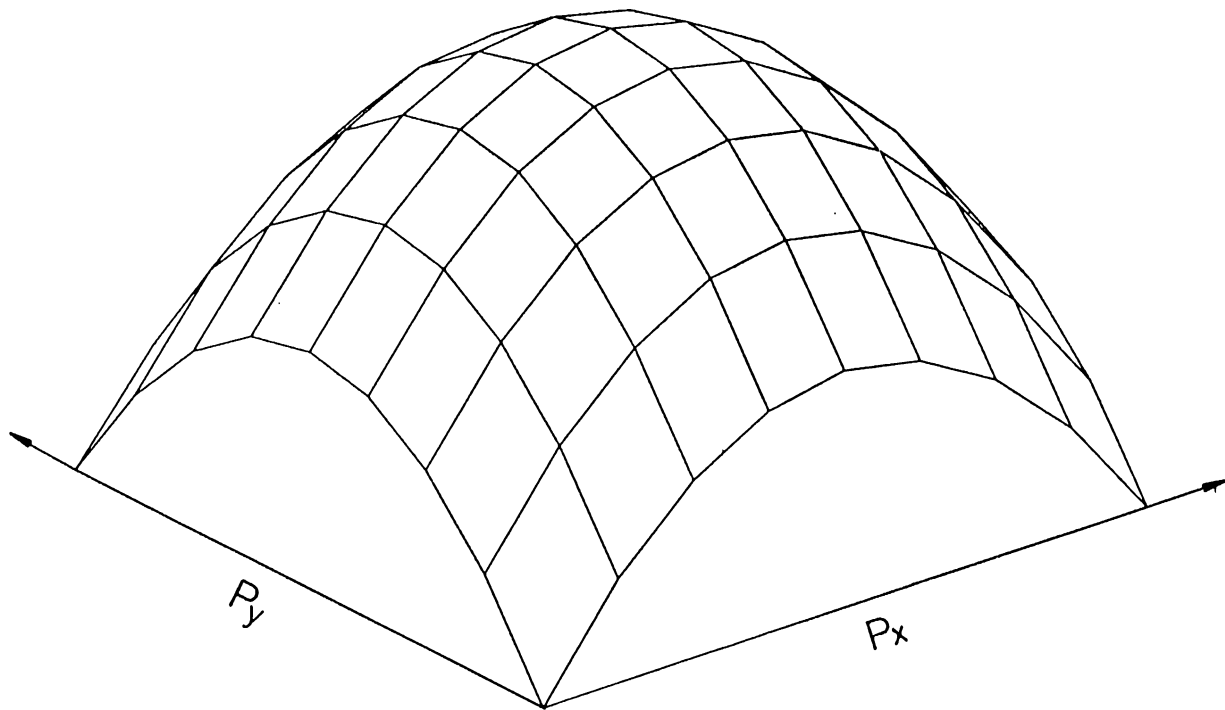


Figure 3.13: Covariance vs $|\bar{p}|$, (\bar{p}' and \bar{p}'_A are fixed, $\bar{p} = \bar{p}_A$, $C_n^2 = 10^{-15}$, $D = 0.2 m$, $\lambda = 550 nm$, $d_2 = 2.052 m$, $z = 5 km$, $\kappa_0 = 2\pi/3$, $\kappa_m = 2960$, and $m = 1/77$)

Chapter 4

CONCLUSION

In this thesis, the mean and the covariance functions of the point spread function (PSF), of a turbulence degraded incoherent imaging system, are determined and interpreted. As far as the previously published literature is concerned, the results obtained throughout this work are original.

In particular, we were unable to find any material on the covariance or variance of a turbulence degraded PSF. A rather old reference exists [1] for the optical transfer function (OTF) of a turbulence degraded imaging system. Since OTF is the Fourier transform of PSF, this result is directly related to our work. For purposes of comparison, the results of the above cited work together with the results of an experiment performed by [2], is compared in Figure 4.1 with the OTF predicted by our theory. In Figure 4.1, the solid line represents the curve obtained by the expressions derived in this thesis, the dotted one is the result derived in [1], and the discrete points indicated by ‘o,+x,*’ are the results of the experiment performed by [2].

As it can be observed, the result predicted by this work is in very good agreement with the experiment. Furthermore, although the particular conditions for which the experimental data in [2] was collected, are not affected by the finite size of the lens, in most situations this is a very important parameter. The theory presented in [1] does not take the finite size of the lens into account.

The main results of this thesis can be summarized as;

- 1) The functional form of mean of PSF is; $a_1 e^{a_2 x^{5/3}}$, where x is the absolute value of the difference between the source (in image plane coordinates) and the

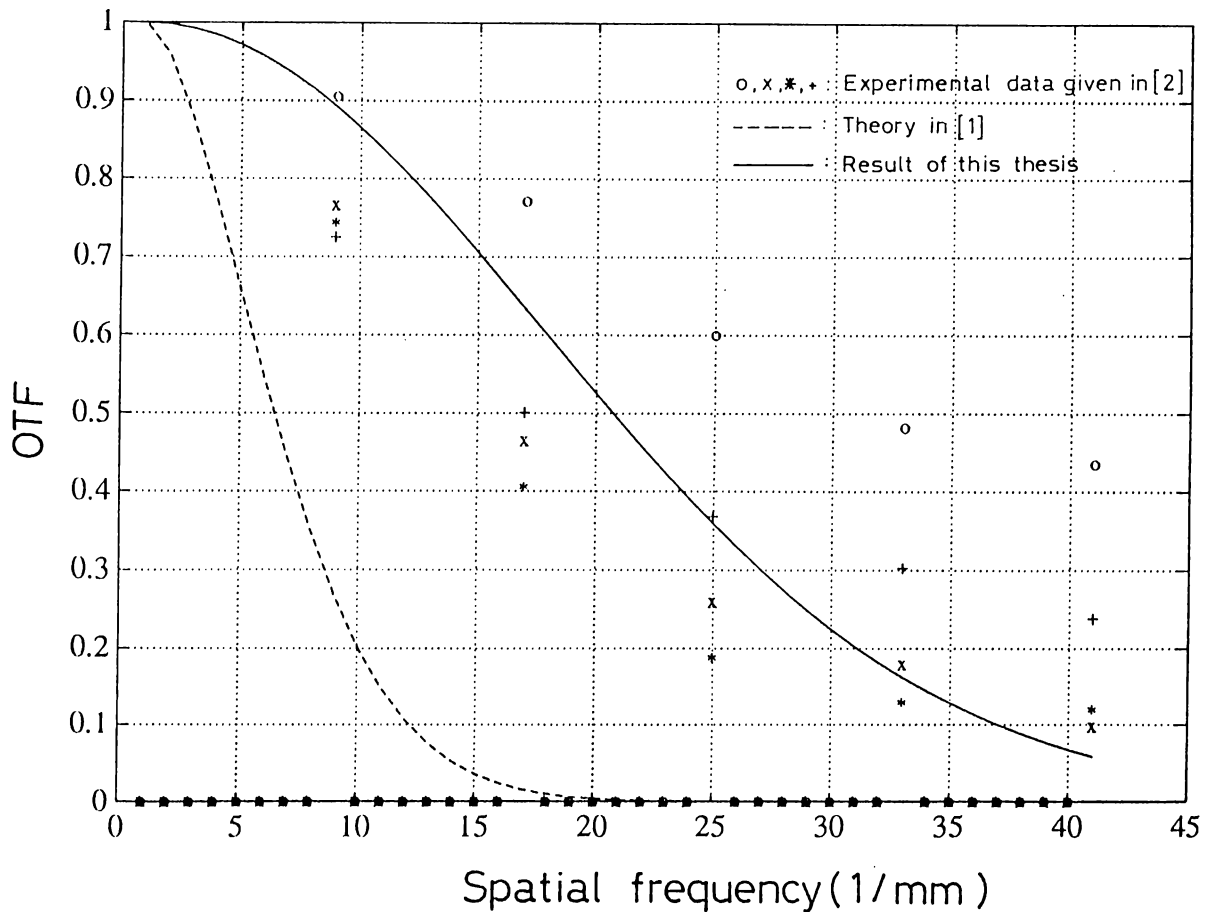


Figure 4.1: OTF versus spatial frequency ($1/mm$), ($height=50m$, $C_n^2 = 4.82 \times 10^{-15} m^{-2/3}$, $\lambda=550nm$, $z=11km$)

observation point. The relationship between the constant a_2 and C_n^2 is stated in section 3.4.

2) The resolution of the system is a function of the strength of the turbulence as well as the diameter of the aperture stop. Increasing the diameter of the aperture stop (which also increases the cost) beyond a predefined value (which is a function of the turbulence strength) gains nothing in terms of the resolution (This result is cited in the literature by many authors).

3) The κ_0 value has significant effect on the resolution of the system. Making κ_0 as large as possible (i.e., decreasing the altitude of the system) improves the resolution with other system parameters remaining unchanged. However, C_n^2 is also highly dependent on elevation, which, combined with the variation in κ_0 , makes the total resolution of the system decrease with increasing elevation above ground.

4) The variance of PSF is maximum at the peak of the mean.

5) The correlation function decreases either when the distance between the image points increase given that the source points are coincident, or when

the distance between source points increase if the image points are coincident, which is consistent with the general behavior of correlation functions.

This thesis can be a starting point of a variety of future research projects. Some of which is listed below;

1) In parallel with increasing computational speed, the expressions given for the variance and covariance of the PSF can be evaluated using a large set of system parameters. Such an extensive set of results would give considerable insight into the behavior of the second order statistics of a PSF.

2) From the point of image processing, the mean and variance results can be used in image reconstruction algorithms. There are a lot of reconstruction techniques for turbulence degraded images one of which is given in [14]. This technique directly requires the results driven in this thesis, since it gives the frequency response of a Wiener filter when the mean and the covariance function of the PSF of an imaging system is known.

3) The effect of polychromatic illumination on the statistics of the PSF may be investigated.

4) A formulation may be investigated for a more straightforward specification of a short exposure PSF statistics.

Appendix A

In this appendix, (2.15) is derived.

Using the change of variables

$$\begin{aligned}\bar{\varepsilon} &= \bar{p}'' - \bar{p}''' \\ \bar{\eta} &= (\bar{p}'' + \bar{p}''')/2\end{aligned}$$

in (2.13) we have,

$$\begin{aligned}E[h_I(\bar{p}, \bar{p}')] &= \int d\bar{\varepsilon} e^{-j\frac{k}{d_2}(\bar{p}-\bar{p}')\cdot\bar{\varepsilon}} e^{-4\pi^2 k^2 z} \int_0^1 dt \int_0^\infty d\kappa \kappa \Phi_n(\kappa) [1 - J_0(t|\bar{\varepsilon}|\kappa)] \\ &\int d\bar{\eta} t_p(\bar{\eta} + \frac{\bar{\varepsilon}}{2}) t_p^*(\bar{\eta} - \frac{\bar{\varepsilon}}{2})\end{aligned}\quad (\text{A.1})$$

For a circular pupil function with diameter D , it is easy to show that,

$$\int d\bar{\eta} t_p(\bar{\eta} + \frac{\bar{\varepsilon}}{2}) t_p^*(\bar{\eta} - \frac{\bar{\varepsilon}}{2}) = \begin{cases} \frac{D^2}{2} [\cos^{-1}(\frac{|\bar{\varepsilon}|}{D}) - \frac{|\bar{\varepsilon}|}{D} \sqrt{1 - (\frac{|\bar{\varepsilon}|}{D})^2}] & \text{if } |\bar{\varepsilon}| < D \\ 0 & \text{otherwise} \end{cases} \quad (\text{A.2})$$

Substituting (A.2) into (A.1), we have,

$$\begin{aligned}E[h_I(\bar{p}, \bar{p}')] &= \pi D^2 \int_0^D d\varepsilon \varepsilon J_0(\frac{2\pi|\bar{p}-\bar{p}'|}{\lambda d_2} \varepsilon) (\cos^{-1} \frac{\varepsilon}{D} - \frac{\varepsilon}{D} \sqrt{1 - (\frac{\varepsilon}{D})^2}) \\ &e^{-4\pi^2 k^2 z} \int_0^1 dt \int_0^\infty d\kappa \kappa \Phi_n(\kappa) [1 - J_0(t\varepsilon\kappa)]\end{aligned}\quad (\text{A.3})$$

Since (A.3) depends only on $|\bar{p} - \bar{p}'|$, it represents a shift invariant impulse response.

Appendix B

In [10] an expression for $E[\Psi_1(\bar{p}, \bar{p}')\Psi_1^*(\bar{p}_A, \bar{p}'_A)]$ has been given. Here, following similar steps as [10] an expression for $E[\Psi_1(\bar{p}, \bar{p}')\Psi_1(\bar{p}_A, \bar{p}'_A)]$ will be derived.

It is shown in [10] that,

$$\Psi_1(\bar{r}, \bar{r}') = \frac{k_0^2}{2\pi U_0(\bar{r}, \bar{r}')} \int d\bar{r}'' n_1(\bar{r}'') U_0(\bar{r}'', \bar{r}') \frac{e^{jk|\bar{r}-\bar{r}''|}}{|\bar{r}-\bar{r}''|} \quad (\text{B.1})$$

where $U_0(\bar{r}'', \bar{r}') = \frac{e^{jk|\bar{r}''-\bar{r}'|}}{|\bar{r}''-\bar{r}'|}$, $n_1(\bar{r}'')$ is the random fluctuations of the refractive index of the atmosphere, and all position vectors are members of a 3-D space. Throughout this thesis, the symbol \bar{r} is used to represent a vector in a 3-D space, whereas \bar{p} is used for a vector in a 2-D plane.

Using (B.1) and invoking the paraxial approximation (B.1) can be written as;

$$\Psi_1(\bar{p}, \bar{p}') = \frac{zk_0^2}{2\pi} e^{-j\frac{k}{2z}(\bar{p}-\bar{p}')^2} \int d\bar{r}'' \frac{n_1(\bar{r}'')}{z''(z-z'')} e^{jk[\frac{(\bar{p}''-\bar{p})^2}{2z''} + \frac{(\bar{p}''-\bar{p}')^2}{2(z-z'')}]} \quad (\text{B.2})$$

where all the position vectors (i.e., \bar{p} , \bar{p}' , \bar{p}_A , \bar{p}'_A) lie on a transverse plane perpendicular to the predominant direction of propagation. The \bar{p}' and \bar{p}'_A vectors are assumed to be on the $z = 0$ plane, and \bar{p} and \bar{p}_A points are assumed to be on a plane located at a distance of z meters from the $z = 0$ plane.

Using (B.2), and assuming that n_1 is a stationary random variable, the expression for $E[\Psi_1(\bar{p}, \bar{p}')\Psi_1(\bar{p}_A, \bar{p}'_A)]$ can be written as;

$$E[\Psi_1(\bar{p}, \bar{p}')\Psi_1(\bar{p}_A, \bar{p}'_A)] = \left(\frac{zk^2}{2\pi}\right)^2 e^{-j\frac{k}{2z}[(\bar{p}-\bar{p}')^2 + (\bar{p}_A-\bar{p}'_A)^2]} \int d\bar{\kappa} Q(\bar{\kappa}) \quad (\text{B.3})$$

As defined in section 1.3, $\bar{\kappa}$ is the wavenumber vector with units of radians per meter, and Q is given by;

$$Q(\bar{\kappa}) = \int d\bar{r}'' \int d\bar{r}''' \frac{F_n(\bar{\kappa}, z''-z''')}{z''z'''(z-z'')(z-z''')} e^{-j\bar{\kappa}\cdot(\bar{p}''-\bar{p}''')} e^{jk[\frac{(\bar{p}''-\bar{p})^2}{2z''} + \frac{(\bar{p}''-\bar{p}')^2}{2(z-z'')} + \frac{(\bar{p}'''-\bar{p}_A)^2}{2z'''} + \frac{(\bar{p}'''-\bar{p}'_A)^2}{2(z-z''')}] } \quad (\text{B.4})$$

where,

$$F_n(\bar{\kappa}, z'' - z''') = \frac{1}{(2\pi)^2} \int d\bar{p}_f B_n(\bar{p}_f, z'' - z''') e^{j\bar{\kappa} \cdot (\bar{p}_f)} \quad (\text{B.5})$$

In (B.5) $B_n(\bar{p}_f, z'' - z''')$ is defined as;

$$B_n(\bar{p}_f, z'' - z''') = B_n(\bar{p}'' - \bar{p}''', z'' - z''') = E[n_1(\bar{r}'') n_1(\bar{r}''')] \quad (\text{B.6})$$

Conforming to the notation introduced in (B.4), z'' and z''' are the components of \bar{r}'' and \bar{r}''' along the direction of propagation, and \bar{p}'' and \bar{p}''' are the components on the transverse plane perpendicular to the direction of propagation.

After evaluating the \bar{p}'' and \bar{p}''' integrals in (B.4) and with some simplification, the Q function turns out to be

$$Q(\bar{\kappa}) = -\left(\frac{2\pi}{kz}\right)^2 e^{j\frac{k}{2z}[(\bar{p}-\bar{p}')^2+(\bar{p}_A-\bar{p}'_A)^2]} \int_0^z dz'' \int_0^z dz''' e^{-j[(\frac{z''}{z}\bar{p}' - \frac{z'''}{z}\bar{p}'_A) \cdot \bar{\kappa} + (\frac{z-z''}{z}\bar{p} - \frac{z-z'''}{z}\bar{p}_A) \cdot \bar{\kappa}]} \\ e^{-j\frac{k}{2kz}[z''(z-z'') + z'''(z-z''')]} \\ F_n(\bar{\kappa}, z'' - z''') \quad (\text{B.7})$$

With the new integral variables defined as,

$$\varepsilon = z'' - z''' \\ \eta = (z'' + z''')/2$$

and neglecting the terms that involve ε in the exponent (because $F_n(\bar{\kappa}, |\varepsilon|)$ is nonzero only when $|\varepsilon|$ is on the order of l , where l is the scale length of the inhomogeneities, and $kl \ll 1$ [10]), the final expression for the Q function comes out to be,

$$Q(\bar{\kappa}) = -\left(\frac{2\pi}{kz}\right)^2 e^{j\frac{k}{2z}[(\bar{p}-\bar{p}')^2+(\bar{p}_A-\bar{p}'_A)^2]} \int_0^z d\eta \int_0^\infty d\varepsilon F_n(\bar{\kappa}, |\varepsilon|) e^{-j[\frac{\eta}{z}\bar{p}_d \cdot \bar{\kappa} - (1-\frac{\eta}{z})\bar{p}'_d \cdot \bar{\kappa}]} \\ e^{-j\frac{k}{k}\frac{\eta^2}{z}(\frac{\eta}{z} - \frac{\eta^2}{z^2})} \quad (\text{B.8})$$

where $\bar{p}'_d = \bar{p}' - \bar{p}'_A$ and $\bar{p}_d = \bar{p} - \bar{p}_A$.

It is given in [6] that

$$\int_0^\infty F_n(\bar{\kappa}, \varepsilon) d\varepsilon = \pi \Phi_n(\bar{\kappa})$$

where $\Phi_n(\bar{\kappa})$ is the spectral density of the index of refraction fluctuations. Using this result, and defining t as $t = \frac{\eta}{z}$, the expression for $E[\Psi_1(\bar{p}, \bar{p}') \Psi_1(\bar{p}_A, \bar{p}'_A)]$ becomes

$$E[\Psi_1(\bar{p}, \bar{p}') \Psi_1(\bar{p}_A, \bar{p}'_A)] = -2\pi k^2 z \int d\bar{\kappa} \Phi_n(\bar{\kappa}) \int_0^1 dt e^{-j[t\bar{p}_d \cdot \bar{\kappa} + (1-t)\bar{p}'_d \cdot \bar{\kappa} + \frac{k}{k} \frac{t^2}{z}(t-t^2)]} \quad (\text{B.9})$$

If n_1 is assumed to be isotropic, (B.9) turns out to be,

$$E[\Psi_1(\bar{p}, \bar{p}')\Psi_1(\bar{p}_A, \bar{p}'_A)] = -4\pi^2 k^2 z \int_0^\infty d\kappa \kappa \Phi_n(\kappa) \int_0^1 dt J_0(|t\bar{p}_d + (1-t)\bar{p}'_d|\kappa) e^{-j\frac{\kappa^2 z}{k}(t-t^2)} \quad (\text{B.10})$$

The expression of $E[\Psi_1(\bar{p}, \bar{p}')\Psi_1^*(\bar{p}_A, \bar{p}'_A)]$ which is given in [10] is also used in this work, so it is restated here for convenience;

$$E[\Psi_1(\bar{p}, \bar{p}')\Psi_1^*(\bar{p}_A, \bar{p}'_A)] = 4\pi^2 k^2 z \int_0^\infty d\kappa \kappa \Phi_n(\kappa) \int_0^1 dt J_0(|t\bar{p}_d + (1-t)\bar{p}'_d|\kappa) \quad (\text{B.11})$$

Appendix C

Here, an expression for the function F ;

$$F = E[e^{\Psi(\bar{p}'', \frac{-\bar{p}'}{m}) + \Psi^*(\bar{p}''', \frac{-\bar{p}'}{m}) + \Psi(\bar{p}'''' , \frac{-\bar{p}'}{m\Delta}) + \Psi^*(\bar{p}'''' , \frac{-\bar{p}'}{m\Delta})}] \quad (C.1)$$

is obtained.

It is known [10] that, if $f = \log(y)$ is a random variable of order n_1 with mean $E[f]$ and mean square $E[f^2]$, than $E[y]$ can be written as,

$$E[y] = e^{E[f] + \frac{1}{2}E[(f-E[f])^2]} \quad (C.2)$$

which is correct through terms of order n_1^2 .

Using (C.2), and the fact that $\Psi = \Psi_1 + \Psi_2$ [Rytov solution], (C.1) can be written as,

$$F = e^{E[\Psi_2(\bar{p}'', \frac{-\bar{p}'}{m}) + \Psi_2^*(\bar{p}''', \frac{-\bar{p}'}{m}) + \Psi_2(\bar{p}'''' , \frac{-\bar{p}'}{m\Delta}) + \Psi_2^*(\bar{p}'''' , \frac{-\bar{p}'}{m\Delta})]} e^{\frac{1}{2}E[(\Psi_1(\bar{p}'', \frac{-\bar{p}'}{m}) + \Psi_1^*(\bar{p}''', \frac{-\bar{p}'}{m}) + \Psi_1(\bar{p}'''' , \frac{-\bar{p}'}{m\Delta}) + \Psi_1^*(\bar{p}'''' , \frac{-\bar{p}'}{m\Delta})]^2]} \quad (C.3)$$

It is stated in [10] that the 1st and 2nd order Rytov solutions are related by;

$$E[\Psi_2] = -E[|\Psi_1|^2] \quad (C.4)$$

Consequently, using (C.4) in (C.3) we have,

$$F = e^{-2E[|\Psi_1|^2]} e^{E[\Psi_1(\bar{p}'', \frac{-\bar{p}'}{m})\Psi_1^*(\bar{p}''', \frac{-\bar{p}'}{m})]} e^{E[\Psi_1(\bar{p}'', \frac{-\bar{p}'}{m})\Psi_1(\bar{p}'''' , \frac{-\bar{p}'}{m\Delta})]} e^{E[\Psi_1(\bar{p}'', \frac{-\bar{p}'}{m})\Psi_1^*(\bar{p}'''' , \frac{-\bar{p}'}{m\Delta})]} e^{E[\Psi_1^*(\bar{p}''', \frac{-\bar{p}'}{m})\Psi_1(\bar{p}'''' , \frac{-\bar{p}'}{m\Delta})]} e^{E[\Psi_1^*(\bar{p}''', \frac{-\bar{p}'}{m})\Psi_1^*(\bar{p}'''' , \frac{-\bar{p}'}{m\Delta})]} e^{E[\Psi_1(\bar{p}'''' , \frac{-\bar{p}'}{m\Delta})\Psi_1^*(\bar{p}'''' , \frac{-\bar{p}'}{m\Delta})]} \quad (C.5)$$

Substituting (B.10) and (B.11) in (C.5) we obtain,

$$F = e^{-4\pi^2 k^2 z} \int_0^1 dt \int_0^\infty d\kappa \kappa \Phi_n(\kappa) f e \quad (C.6)$$

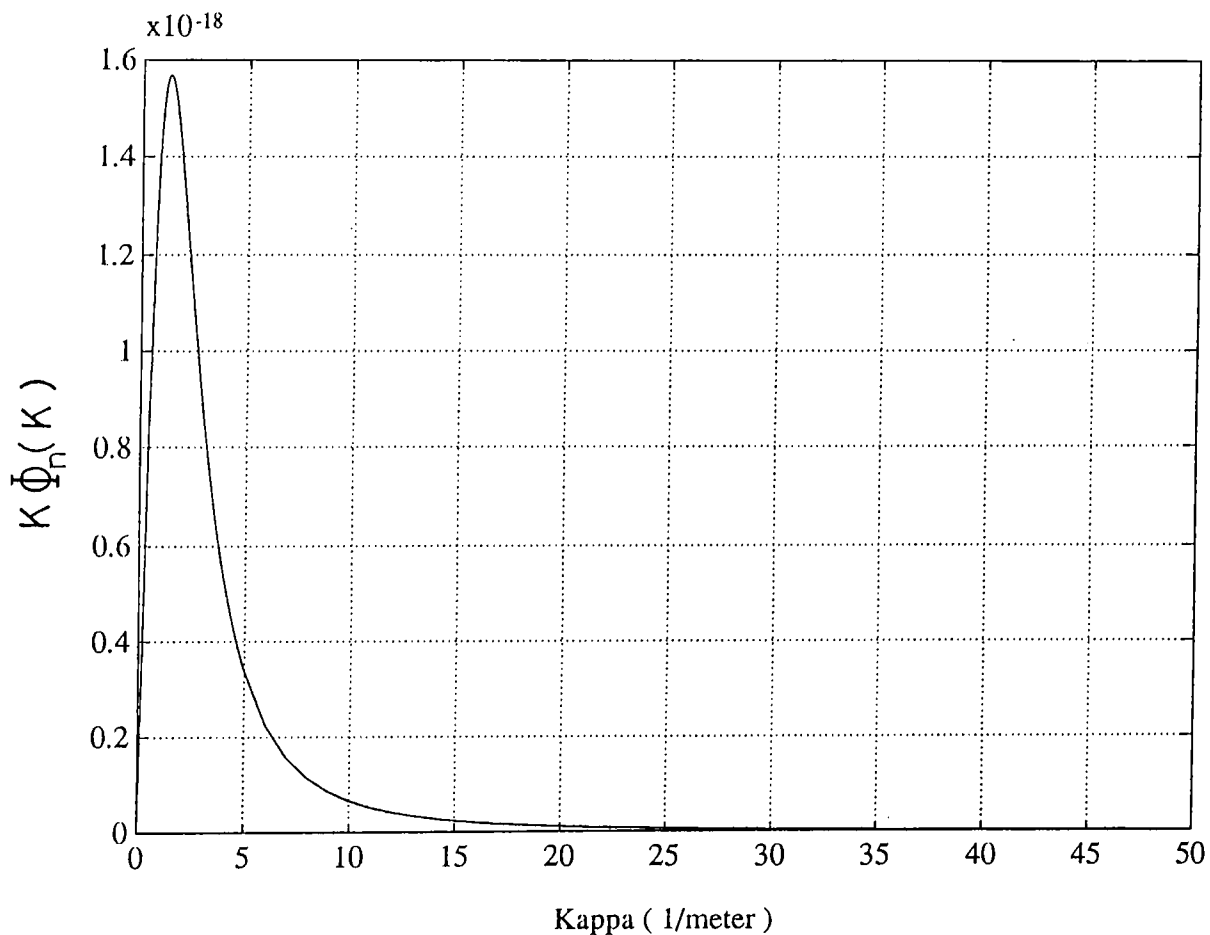


Figure C.1: $\kappa\Phi_n(\kappa)$ versus κ ($C_n^2 = 10^{-15} m^{-2/3}$, $D = 0.2 m$, $\lambda = 550 nm$, $d_2 = 2.052 m$, $z = 5 km$, $\kappa_0 = 2\pi/3$, $\kappa_m = 2960$, and $m = 1/77$)

where

$$\begin{aligned}
f_e = & 2 - J_0(t|\bar{p}'' - \bar{p}'''|\kappa) - J_0(t|\bar{p}'''' - \bar{p}'''''|\kappa) \\
& + J_0(|\frac{\bar{p}' - \bar{p}'_\Delta}{m}(t-1) + t(\bar{p}'' - \bar{p}''''')|\kappa)e^{-j\frac{z}{k}(t-t^2)\kappa^2} \\
& - J_0(|\frac{\bar{p}' - \bar{p}'_\Delta}{m}(t-1) + t(\bar{p}'' - \bar{p}''''')|\kappa) \\
& - J_0(|\frac{\bar{p}' - \bar{p}'_\Delta}{m}(t-1) + t(\bar{p}''' - \bar{p}''''')|\kappa) \\
& + J_0(|\frac{\bar{p}' - \bar{p}'_\Delta}{m}(t-1) + t(\bar{p}''' - \bar{p}''''')|\kappa)e^{j\frac{z}{k}(t-t^2)\kappa^2} \tag{C.7}
\end{aligned}$$

At this point we will use some approximations to simplify the above equation. Figure C.1 shows $\kappa\Phi_n(\kappa)$ as a function of κ . As it is seen, for $\kappa > 20$ this function becomes very close to zero. Consequently,

$$E_d = \frac{z}{k}(t - t^2)\kappa^2 \tag{C.8}$$

has its maximum value E_d^{max} when $t = \frac{1}{2}$ and $\kappa = 20$;

$$E_d^{max} = \frac{z\lambda}{2\pi} \frac{1}{4} 400 \tag{C.9}$$

When $L_d^{max} < 0.1$, the exponential terms that appear in the 2nd and the last terms of (C.7) has no effect. Thus, they can be taken as unity if the following condition is met;

$$\frac{z\lambda}{2\pi} 100 < 0.1 \Rightarrow \lambda z < 2\pi 10^{-3} \quad (\text{C.10})$$

For optical frequencies this restriction can easily be met for all practical propagation distances z . Hence, the exponential terms in (C.7) can be neglected. Thus we have,

$$\begin{aligned} f_e = & 2 - J_0(t|\bar{p}'' - \bar{p}'''|\kappa) - J_0(t|\bar{p}'''' - \bar{p}''''|\kappa) \\ & + J_0(|\frac{\bar{p}' - \bar{p}'\Delta}{m}(t-1) + t(\bar{p}'' - \bar{p}'''')|\kappa) \\ & - J_0(|\frac{\bar{p}' - \bar{p}'\Delta}{m}(t-1) + t(\bar{p}'' - \bar{p}'''')|\kappa) \\ & - J_0(|\frac{\bar{p}' - \bar{p}'\Delta}{m}(t-1) + t(\bar{p}''' - \bar{p}'''')|\kappa) \\ & + J_0(|\frac{\bar{p}' - \bar{p}'\Delta}{m}(t-1) + t(\bar{p}''' - \bar{p}'''')|\kappa) \end{aligned} \quad (\text{C.11})$$

which together with (C.6) provides an analytical expression for (C.1).

Appendix D

In this appendix, a polynomial fit to the function $I(\bar{\alpha}, \bar{\beta})$ defined in (2.20) is derived.

Let

$$I' = \int_0^1 dt g'[\gamma(t)] \quad (\text{D.1})$$

where

$$g'[\gamma(t)] = \sum_{i=1}^5 \frac{-2r_i p_i}{[\gamma(t)]^2 + p_i^2} \quad (\text{D.2})$$

Substituting $\gamma(t) = |\bar{\alpha}t + \bar{\beta}|\kappa_0$ into (D.2), the expression for I' turns out to be,

$$I' = \sum_{i=1}^5 \int_0^1 dt \frac{-2r_i p_i}{t^2 |\bar{\alpha}|^2 \kappa_0^2 + 2t(\bar{\alpha} \cdot \bar{\beta}) \kappa_0^2 + |\bar{\beta}|^2 \kappa_0^2 + p_i^2} \quad (\text{D.3})$$

The t integral in (D.3) can be calculated, and (D.1) can be written as,

$$I' = \begin{cases} \sum_{i=1}^5 \frac{-2r_i p_i}{|\bar{\beta}|^2 \kappa_0^2 + p_i^2} & \text{if } \bar{\alpha} = 0 \\ \sum_{i=1}^5 \frac{-2r_i p_i}{d} [\tan^{-1}(\frac{|\bar{\alpha}|^2 \kappa_0^2 + (\bar{\alpha} \cdot \bar{\beta}) \kappa_0^2}{d}) - \tan^{-1}(\frac{(\bar{\alpha} \cdot \bar{\beta}) \kappa_0^2}{d})] & \text{if } \bar{\alpha} \neq 0 \end{cases} \quad (\text{D.4})$$

where

$$d = \sqrt{|\bar{\alpha}|^2 \kappa_0^2 (|\bar{\beta}|^2 \kappa_0^2 + p_i^2) - (\bar{\alpha} \cdot \bar{\beta})^2 \kappa_0^4}$$

Finally,

$$I_f(\bar{\alpha}, \bar{\beta}) = \frac{0.033 C_n^2}{\kappa_0^{5/3}} I'(\bar{\alpha}, \bar{\beta}) \quad (\text{D.5})$$

is the desired numerical fit to $I(\bar{\alpha}, \bar{\beta})$ whose coefficients are,

$$r_1 = -0.2578, p_1 = -4.6881$$

$$r_2 = 0.3908, p_2 = -1.8562$$

$$r_3 = 0.0967, p_3 = -0.8786$$

$$r_4 = 0.0091, p_4 = -0.2831$$

$$r_5 = 0.0001, p_5 = -0.0458$$

With these coefficients, the error (defined as $|\frac{I(\bar{\alpha}, \bar{\beta}) - J_I(\bar{\alpha}, \bar{\beta})}{I(\bar{\alpha}, \bar{\beta})}|$) is at most on the order of $\frac{0.933C^2}{\kappa_0^{5/3}} 10^{-4}$ which is quite acceptable.

Appendix E

In this appendix, the correlation function (2.16);

$$E[h_I(\bar{p}, \bar{p}')h_I(\bar{p}_\Lambda, \bar{p}'_\Lambda)] = \int d\bar{p}'' \int d\bar{p}''' \int d\bar{p}'''' \int d\bar{p}''''' e^{-j\frac{k}{\alpha_2}[(\bar{p}-\bar{p}')\cdot(\bar{p}''-\bar{p}''')+(\bar{p}_\Lambda-\bar{p}'_\Lambda)\cdot(\bar{p}''''-\bar{p}''''')]} t_p(\bar{p}'')t_p^*(\bar{p}''')t_p(\bar{p}''''')t_p^*(\bar{p}''''')I^r \quad (\text{E.1})$$

is modified for the sake of increasing the speed of the numerical calculations.

The expression for the function I^r was given in (2.18);

$$I^r = e^{-4\pi^2 k^2 z} \int_0^1 dt \int_0^\infty d\kappa \kappa \Phi_n(\kappa) f_e \quad (\text{E.2})$$

where

$$\begin{aligned} f_e = & 2 - J_0(t|\bar{p}'' - \bar{p}'''|\kappa) - J_0(t|\bar{p}'''' - \bar{p}'''''\kappa) \\ & + J_0(|\frac{\bar{p}' - \bar{p}'_\Lambda}{m}(t-1) + t(\bar{p}'' - \bar{p}''''')|\kappa) \\ & - J_0(|\frac{\bar{p}' - \bar{p}'_\Lambda}{m}(t-1) + t(\bar{p}'' - \bar{p}''''')|\kappa) \\ & - J_0(|\frac{\bar{p}' - \bar{p}'_\Lambda}{m}(t-1) + t(\bar{p}''' - \bar{p}''''')|\kappa) \\ & + J_0(|\frac{\bar{p}' - \bar{p}'_\Lambda}{m}(t-1) + t(\bar{p}''' - \bar{p}''''')|\kappa) \end{aligned} \quad (\text{E.3})$$

In the above expression, each integral variable has one x and one y component, which are in the range $[-\frac{D}{2}, \frac{D}{2}]$, where D is the diameter of the pupil.

Changing the integral variables;

$$\begin{aligned} \bar{\varepsilon}_1 &= \bar{p}'' - \bar{p}''' \\ \bar{\eta}_1 &= (\bar{p}'' + \bar{p}''')/2 \\ \bar{\varepsilon}_2 &= \bar{p}'''' - \bar{p}'''''' \\ \bar{\eta}_2 &= (\bar{p}'''' + \bar{p}''''')/2 \end{aligned} \quad (\text{E.4})$$

and defining new integral variables only for $\bar{\eta}_1$ and $\bar{\eta}_2$ as,

$$\begin{aligned} \bar{u} &= \bar{\eta}_1 - \bar{\eta}_2 \\ \bar{v} &= (\bar{\eta}_1 + \bar{\eta}_2)/2 \end{aligned} \quad (\text{E.5})$$

the following expression for (E.1) is obtained;

$$E[h_I(\bar{p}, \bar{p}')h_I(\bar{p}_\Lambda, \bar{p}'_\Lambda)] = \int d\bar{\varepsilon}_1 \int d\bar{\varepsilon}_2 \int d\bar{u} e^{-j\frac{k}{a_2}[(\bar{p}-\bar{p}')\cdot\bar{\varepsilon}_1+(\bar{p}_\Lambda-\bar{p}'_\Lambda)\cdot\bar{\varepsilon}_2]} T_p I' \quad (\text{E.6})$$

where

$$I' = e^{-4\pi^2 k^2 z} \int_0^1 dt \int_0^\infty d\kappa \kappa \Phi_n(\kappa) f'_c \quad (\text{E.7})$$

$$\begin{aligned} f'_c = & 2 - J_0(t|\bar{\varepsilon}_1|\kappa) - J_0(t|\bar{\varepsilon}_2|\kappa) \\ & + J_0\left(\left|\frac{\bar{p}'-\bar{p}'_\Lambda}{m}(t-1) + t\left(\bar{u} + \frac{\bar{\varepsilon}_1-\bar{\varepsilon}_2}{2}\right)\right|\kappa\right) \\ & - J_0\left(\left|\frac{\bar{p}'-\bar{p}'_\Lambda}{m}(t-1) + t\left(\bar{u} + \frac{\bar{\varepsilon}_1+\bar{\varepsilon}_2}{2}\right)\right|\kappa\right) \\ & - J_0\left(\left|\frac{\bar{p}'-\bar{p}'_\Lambda}{m}(t-1) + t\left(\bar{u} - \frac{\bar{\varepsilon}_1+\bar{\varepsilon}_2}{2}\right)\right|\kappa\right) \\ & + J_0\left(\left|\frac{\bar{p}'-\bar{p}'_\Lambda}{m}(t-1) + t\left(\bar{u} - \frac{\bar{\varepsilon}_1-\bar{\varepsilon}_2}{2}\right)\right|\kappa\right) \end{aligned} \quad (\text{E.8})$$

and

$$T_p = \int d\bar{v} t_p\left(\bar{v} + \frac{\bar{u}}{2} + \frac{\bar{\varepsilon}_1}{2}\right) t_p^*\left(\bar{v} + \frac{\bar{u}}{2} - \frac{\bar{\varepsilon}_1}{2}\right) t_p\left(\bar{v} - \frac{\bar{u}}{2} + \frac{\bar{\varepsilon}_2}{2}\right) t_p^*\left(\bar{v} - \frac{\bar{u}}{2} - \frac{\bar{\varepsilon}_2}{2}\right) \quad (\text{E.9})$$

In (E.6) the x and y components of $\bar{\varepsilon}_1$ and $\bar{\varepsilon}_2$ (i.e., $\varepsilon_{1x}, \varepsilon_{2x}, \varepsilon_{1y}, \varepsilon_{2y}$) are between $-D$ and D , the x component of \bar{u} (i.e., u_x) is between $-[r(\varepsilon_{1x}) + r(\varepsilon_{2x})]$ and $[r(\varepsilon_{1x}) + r(\varepsilon_{2x})]$ and the y component of \bar{u} (i.e., u_y) is between $-[r(\varepsilon_{1y}) + r(\varepsilon_{2y})]$ and $[r(\varepsilon_{1y}) + r(\varepsilon_{2y})]$ where

$$r(u) = \frac{D - |u|}{2}$$

Referring to (E.9), the range for the x component of \bar{v} (i.e., v_x) is given below. To find the range for the y component, just change the x indices to y 's.

If $r(\varepsilon_{1x}) > r(\varepsilon_{2x})$:

$$u_x \in [r(\varepsilon_{1x}) + r(\varepsilon_{2x}), r(\varepsilon_{1x}) - r(\varepsilon_{2x})] \Rightarrow v_x \in \left[-r(\varepsilon_{2x}) + \frac{u_x}{2}, r(\varepsilon_{1x}) - \frac{u_x}{2}\right]$$

$$u_x \in [r(\varepsilon_{1x}) - r(\varepsilon_{2x}), r(\varepsilon_{2x}) - r(\varepsilon_{1x})] \Rightarrow v_x \in \left[-r(\varepsilon_{2x}) + \frac{u_x}{2}, r(\varepsilon_{2x}) + \frac{u_x}{2}\right]$$

$$u_x \in [r(\varepsilon_{2x}) - r(\varepsilon_{1x}), -r(\varepsilon_{2x}) - r(\varepsilon_{1x})] \Rightarrow v_x \in \left[-r(\varepsilon_{1x}) - \frac{u_x}{2}, r(\varepsilon_{2x}) + \frac{u_x}{2}\right]$$

If $r(\varepsilon_{1x}) \leq r(\varepsilon_{2x})$:

$$u_x \in [r(\varepsilon_{1x}) + r(\varepsilon_{2x}), r(\varepsilon_{2x}) - r(\varepsilon_{1x})] \Rightarrow v_x \in \left[-r(\varepsilon_{2x}) + \frac{u_x}{2}, r(\varepsilon_{1x}) - \frac{u_x}{2}\right]$$

$$u_x \epsilon [r(\epsilon_{2x}) - r(\epsilon_{1x}), r(\epsilon_{1x}) - r(\epsilon_{2x})] \Rightarrow v_x \epsilon [-r(\epsilon_{1x}) - \frac{u_x}{2}, r(\epsilon_{1x}) - \frac{u_x}{2}]$$

$$u_x \epsilon [r(\epsilon_{1x}) - r(\epsilon_{2x}), -r(\epsilon_{1x}) - r(\epsilon_{2x})] \Rightarrow v_x \epsilon [-r(\epsilon_{1x}) - \frac{u_x}{2}, r(\epsilon_{2x}) + \frac{u_x}{2}]$$

In order to numerically evaluate the expression for the correlation function, the $\bar{\epsilon}_1$, $\bar{\epsilon}_2$ and \bar{u} integrals of (E.6) were approximated by 11×11 points, and \bar{v} integral was approximated by 15×15 points.

REFERENCES

- [1] R.E.Hufnagel and N.R.Stanley, *Modulation Transfer Function Associated with Image Transmission Through Turbulent Media*, J.Opt.Soc.Am, 1964, vol:54, No:1, 52-61
- [2] E. Djurle and A.Bäck, J.Opt.Soc.Am, 1961, vol:51, 1029
- [3] R.F.Lutomirski and H.T.Yura, *Imaging of Extended Objects Through a Turbulent Atmosphere*, Applied Optics, 1974, vol:13, No:2, 431-437
- [4] Joseph W.Goodman, *Statistical Optics*, John Wiley and Sons, 1985
- [5] Jeffrey H. Shapiro, *Diffraction-Limited Atmospheric Imaging of Extended Objects*, J.Opt.Soc.Am, 1976, vol:66, No:5, 469-477
- [6] V.I.Tatarski, *Wave Propagation in a Turbulent Medium*, McGraw-Hill, 1961
- [7] John W. Strohbehn, *Laser Beam Propagation in the Atmosphere*, Springer-Verlag, 1978
- [8] Akira Ishimaru, *Wave Propagation and Scattering in Random Media*, vol:2, Academic Press, 1978
- [9] Ronald L. Fante, *Electromagnetic Beam Propagation in Turbulent Media*, Proceeding of the IEEE, 1975, vol:63, No:12, 1669-1692
- [10] H.T.Yura, *Mutual Coherence Function of a Finite Cross Section Optical Beam Propagating in a Turbulent Medium*, Applied Optics, 1972, vol:11, No:6, 1399-1406
- [11] R.F.Lutomirski and H.T.Yura, *Modulation-Transfer Function and Phase-Structure Function of an Optical Wave in a Turbulent Medium*, Letters to the Editor, 1969, 999-1000
- [12] H.T.Yura *Optical Propagation through a Turbulent Medium*, Letters to the Editor, 1969, 111-112

- [13] , Keigo Iizuka, *Engineering Optics*, Springer-Verlag, 1983
- [14] David Slepian, *Linear Least-Squares Filtering of Distorted Images*,
J.Opt.Soc.Am, 1967, vol:57, No:7, 918-922